Mon. Not. R. Astron. Soc. **000**, 1–21 (2009) Printed 23 March 2009 (MN LATEX style file v2.2)

Strong $z \sim 0.5$ O VI Absorption Toward PKS 0405-123: Implications for Ionization and Metallicity of the Cosmic Web⋆

J. Christopher Howk,[2] Joseph S. Ribaudo,[2] Nicolas Lehner,[2]
J. Xavier Prochaska,[3] Hsiao-Wen Chen[4]
[2]*Department of Physics, University of Notre Dame, Notre Dame, IN, USA*
[3] *UCO/Lick Observatory; University of California, Santa Cruz; Santa Cruz, CA, USA*
[4]*Department of Astronomy & Astrophysics, University of Chicago, Chicago, IL 60637*

Accepted XXX. Received XXX.

ABSTRACT

We present observations of the intervening O VI absorption line system at $z_{abs} = 0.495096$ toward the QSO PKS 0405–123 ($z_{em} = 0.5726$) obtained with the *Far Ultraviolet Spectroscopic Explorer* and Space Telescope Imaging Spectrograph on board the *Hubble Space Telescope*. In addition to strong O VI, with $\log N(\mathrm{O\ VI}) = 14.47 \pm 0.02$, and moderate H I, with $\log N(\mathrm{H\ I}) = 14.29 \pm 0.10$, this absorber shows absorption from C III, N IV, O IV, and O V, with upper limits for another seven ions. The large number of available ions allows us to test ionization models usually adopted with far fewer contraints. We find that the observed ionic column densities cannot be matched by single temperature collisional ionization models, in or out of equilibrium. Photoionization models can match all of the observed column densities, including O VI. If one assumes photoionization by a UV background dominated by QSOs, the metallicity of the gas is [O/H]≈ -0.15, while if one assumes a model for the UV background with contributions from ionizing photons escaping from galaxies the metallicity is [O/H]≈ -0.62. Both give [N/O]~ -0.6 and [C/H]~ -0.2 to ~ -0.1, though a solar C/O ratio is not ruled out. The choice of ionizing spectrum is poorly constrained and leads to systematic abundance uncertainties of ≈ 0.5 dex, despite the wide range of available ions. Multiphase models with a contribution from both photoionized gas (at $T \sim 10^4$ K) and collisionally ionized gas (at $T \sim (1-3) \times 10^5$ K) can also match the observations for either assumed UV background giving very similar metallicities. The O VI in this system is not necessarily a reliable tracer of WHIM matter given the ambiguity in its origins. We do not detect Ne VIII or Mg X absorption. The limit on Ne VIII/ O VI< 0.21 (3σ), the lowest yet observed. Thus this absorber shows no firm evidence of the "warm-hot intergalactic medium" at $T \sim (0.5-3) \times 10^6$ K thought to contain a significant fraction of the baryons at low redshift. We present limits on the total column of warm-hot gas in this absorber as a function of temperature. This system would be unlikely to provide detectable X-ray absorption in the ions O VII or O VIII even if it resided in front of the brighter X-ray sources in the sky.

Key words: intergalactic medium – quasars: absorption lines – quasars: individual (PKS 0405–123)

1 INTRODUCTION

The baryon density of the universe, Ω_b, is a fundamental quantity in cosmology, and identifying the location and physical state of the baryons is a focus of significant work (see Prochaska & Tumlinson 2008 for a recent review). A census of luminous, emitting baryons in the universe falls short of the total baryon density of the universe determined from other means. Various methods of calculating the baryon density are in good agreement, including the comparison of primordial deuterium measurements with Big Bang nucleosynthesis (e.g., O'Meara et al. 2006, Kirkman et al. 2003), and cosmic mi-

⋆ Based on observations made with the NASA-CNES-CSA Far Ultraviolet Spectroscopic Explorer. FUSE is operated for NASA by the Johns Hopkins University under NASA contract NAS5-32985. Also based on observations made with the NASA/ESA Hubble Space Telescope, obtained from the Data Archive at the Space Telescope Science Institute, which is operated by the Association of Universities for Research in Astronomy, Inc., under NASA contract NAS 5-26555. These observations are associated with program #7576.

crowave background studies with the new WMAP measurements (e.g., Spergel et al. 2006). At high redshift, baryonic matter traced in emission falls short of the total baryon budget because most of the baryons reside and can be found within the cool, photoionized intergalactic medium (IGM) of the Lyα forest (LAF; e.g., Rauch et al. 1997). At lower redshift, $z \lesssim 0.5$, the census of stars and gas in galaxies, galaxies and gas in clusters, etc. still falls short of Ω_b, as emphasized by a number of researchers (Persic & Salucci 1992; Fukugita, Hogan, & Peebles 1998). This baryon deficit persists even if the cool, photoionized LAF is included. The emitting components contribute only $\sim 0.1\Omega_b$ (Prochaska & Tumlinson 2008), while including the LAF may increase this to $\sim 0.3\Omega_b$ (e.g., Danforth & Shull 2008, Lehner et al. 2007, Penton, Stocke, & Shull 2004), though with significant uncertainty.

Thus, the easy to identify baryonic constituents of the low-redshift universe represent $\lesssim 50\%$ of the total baryon budget. Fukugita et al. (1998) suggested that hot gas in the halos of galaxies and in groups of galaxies might help solve this "missing baryons problem." An additional component of the baryon budget was suggested by numerical cosmological simulations, in which Ω_b is an initial condition. Such efforts (e.g., Cen & Ostriker 1999, Davé et al. 2001) pointed out that the mass scale of structures in the universe grows with time, and gas falling into these structures at low redshift might then be heated to quite high temperatures. These works suggested that a significant fraction of the low-redshift baryons might then be found in a "warm-hot intergalactic medium" (WHIM) at tempertures $T \approx 10^{5-7}$ K and densities peaked at ~ 10 times the mean density (e.g., Cen & Ostriker 2006). A comparison of a range of models suggests the WHIM is a robust prediction of modern simulations, which predict $30\% - 50\%$ of the low-redshift baryons might be found in this phase of the IGM (Cen & Ostriker 2006, Davé et al. 2001). More recent numerical and analytical works have supported this general conclusion while exploring the effects of feedback (e.g., from galactic winds), non-equilibrium ionization, and cooling on these predictions and their connection to observables (e.g., Oppenheimer & Davé 2009, Cen & Ostriker 2006, Cen & Fang 2006, Kang et al. 2005, Furlanetto et al. 2005, Fang & Bryan 2001, Phillips et al. 2001, Cen et al. 2001).

Given the low densities and high temperatures predicted for the WHIM, the gas in this phase is difficult to detect in emission or absorption. One approach to studying the baryon content of the WHIM is to identify broad Lyα absorption in the low-z IGM. Tripp et al. (2001), Richter et al. (2004), Sembach et al. (2004), and Lehner et al. (2007) report on the detection of broad Lyα absorbers (BLAs) having $b \gtrsim 40$ km s^{-1}, which corresponds to $T \gtrsim 10^5$ K if thermal broadening predominates. Lehner et al. (2007) conclude the fraction of LAF clouds categorized as BLAs is higher at low-z than at larger redshifts (from the sample of Kirkman & Tytler 1997), consistent with predictions of cosmological simulations if thermal motions dominate the broadening (see Davé et al. 2001). Some of the BLAs may be blends of narrow lines (or even small ripples in the observed QSO continuum), a contamination that is difficult to assess with the generally low signal-to-noise data available with STIS observations. In one case, Richter et al. (2004) find O VI absorption associated with a BLA for which the ratio of O VI to H I b-values is consistent with pure thermal broadening, strongly suggesting an origin within hot gas at $T \sim 3 \times 10^5$ K and supporting the idea that some BLAs are thermally broadened. Similarly, Tripp et al. (2001) identified a blended, broad Lyα line with associated O VI absorption; a joint analysis assuming the H I and O VI arise from the same gas yields $T \sim 2 \times 10^5$ K.

In addition to broad H I absorption, absorption lines from highly-ionized metals may be useful for probing WHIM gas at $T \gtrsim 10^5$ K in filaments or groups (e.g., Verner et al. 1994b, Mulchaey et al. 1996, Cen & Ostriker 1999). The highly ionized stages of oxygen, the most abundant metal, are the best studied, including O VI, O VII, and O VIII. O VII and O VIII have transitions accessible to X-ray instruments, as does O VI. Searches for such absorbers have been hampered by the relatively poor resolution of modern X-ray instruments and the small number of sources observable at high enough signal to noise by the *Chandra* and *XMM-Newton* observatories (see recent summaries by Bregman 2007 and Richter et al. 2008). While a number of measurements have been presented in the literature (e.g., Nicastro et al. 2005), some results are questioned by other analyses (Rasmussen et al. 2007, Kaastra et al. 2006) while a few may be on firmer ground (e.g., Fang et al. 2007). It is thus far difficult to judge the fidelity of the X-ray measurements.

Given the high resolution and sensitivity of the currently-available ultraviolet spectrographs, searches for absorption due to the O VI $1031, 1037$ Å doublet may represent the most efficient means of probing the WHIM, even though O VI is not the dominant ionization state of oxygen for the temperature at which the majority of the WHIM is thought to exist ($\sim 10^6$ K; Davé et al. 2001). The first blind search for low-redshift O VI absorbers (mostly over $0.6 \lesssim z \lesssim 1.3$) of Burles & Tytler (1996) was only sensitive to very strong absorbers but nonetheless demonstrated that these absorbers could trace a significant component of the baryonic mass in the universe. Tripp and collaborators first identified a number of O VI absorption line systems at very low redshift ($z < 0.3$) with the *Far Ultraviolet Spectroscopic Explorer* (*FUSE*) and the Space Telescope Imaging Spectrograph (STIS) on board the *Hubble Space Telescope* (*HST*); though their statistical sample was small, these observations suggested a large number density of O VI absorbers at low-z (Tripp, Savage, & Jenkins 2000; Tripp & Savage 2000). Recent surveys of O VI absorption at low redshift using a complete sample of STIS observations continue to find a very large population of absorbers (Tripp et al. 2008, Thom & Chen 2008a, Danforth & Shull 2008). The number density of intervening O VI absorbers per unit redshift is $dN_{\rm O\,VI}/dz \approx 10 - 20$ for equivalent widths $W_r(\lambda 1031) > 30$ mÅ, perhaps increasing to $dN_{\rm O\,VI}/dz \sim 40$ for $W_r(\lambda 1031) > 10$ mÅ (Danforth & Shull 2008). For comparison, recent estimates for the number density of H I absorbers at $z < 0.4$ give $dN_{\rm H\,I}/dz \approx 95$ for $W_r(\lambda 1215) > 90$ mÅ (Lehner et al. 2007) and ≈ 130 for $W_r(\lambda 1215) > 30$ mÅ (Danforth & Shull 2008). The large number of absorbers by itself suggests that the gas probed by these O VI transitions could indeed be an important reservoir of baryons, although accurate estimates of the ionization state and metallicity of these absorbers are required for a quantitative measure of the total mass density.

However, it is possible or even likely that a significant fraction of O VI absorbers do not trace the WHIM, but rather probe metal-enriched, photoionized IGM material. This point has been emphasized in a number of analyses of individual absorbers and sight lines (Savage et al. 2002, Prochaska et al. 2004, Lehner et al. 2006, Tripp et al. 2006, Cooksey et al. 2008), as well as in recent surveys (Tripp et al. 2008, Thom & Chen 2008b). Oppenheimer & Davé (2009) have recently presented cosmological simulations in which O VI absorbers predominantly trace gas at temperatures $\log T \approx 4.2$, well below the majority of the gas associated with the WHIM. A significant amount of the most commonly-used probe of WHIM gas, O VI, may therefore arise in photoionized gas, although Kang et al. (2005) and Oppenheimer & Davé (2009) have argued that some of the photoionized O VI may be WHIM gas that

has cooled to low temperatures. It remains to be seen, however, if the relatively extreme predictions of Oppenheimer & Davé (2009) will be verified by other simulations.

Undoubtedly some O VI systems are associated with photoionized gas, though whether they outnumber or dominate the WHIM absorbers is a question open to debate (e.g., Danforth 2009). Even if photoionized absorbers represent a significant fraction of the total, most simulations suggest that the highest equivalent width O VI systems are most likely to be collisionally ionized, either tracing WHIM gas or gas associated with the hot halos of galaxies (Cen et al. 2001, Fang & Bryan 2001, Ganguly et al. 2008, Oppenheimer & Davé 2009).

While O VI may not be a perfect tracer of the WHIM, and X-ray measurements are not yet secure, observations of EUV transitions that are redshifted into the bands of *FUSE* and *HST* provide other evidence for shock-heated hot gas in the low-z IGM. In particular, the doublets of Ne VIII $\lambda\lambda$770.409, 780.324, Mg X $\lambda\lambda$609.790, 624.950, and Si XII $\lambda\lambda$499.406, 520.665 are potentially useful probes of hot gas in redshifted IGM (e.g., Verner, Tytler, & Barthel 1994b[1]) or intragroup (Mulchaey et al. 1996) material; these ions peak in abundance in collisional ionization equilibrium at temperatures of $T \approx 6 \times 10^5,\ 1.2 \times 10^6$, and 2×10^6 K, respectively (Gnat & Sternberg 2007). Given the large energies required to produce these ions, they should represent good probes of hot, collisionally ionized gas. They probe temperatures in the same range as X-ray absorption lines, but at better sensitivity to a given H column density given the maturity of the UV instruments with which they can be detected. Savage et al. (2005) have reported on a detection of intervening Ne VIII at $z \approx 0.21$ that they show comes from hot gas. The Ne VIII-bearing gas is part of a multiphase[2] absorber with strong O VI in addition to complex low-ion absorption. The ratio of integrated column densities in this absorber is $N(\text{Ne VIII})/N(\text{O VI}) = 0.33 \pm 0.10$, which is consistent with gas in colllisional ionization equilibrium near $T \approx 5 \times 10^5$ K. Searches for Ne VIII absorption associated with 10 other O VI absorbers have thus far yielded no further detections (Prochaska et al. 2004, Richter et al. 2004, Lehner et al. 2006). However, most of the O VI absorbers are much weaker than that discussed by Savage et al., and in only three of these non-detections is the limit $N(\text{Ne VIII})/N(\text{O VI}) < 0.5$. Thus, Ne VIII has not yet been the subject of a comprehensive search (see limits on dN/dz in Prochaska et al. 2004). To date, however, most Ne VIII searches have used O VI-based searches; if the two ions do not coexist because the WHIM is quite hot, this may not be the best approach.

Here we present a detailed analysis of the ionization state and chemical abundances of the strong O VI absorber at $z = 0.495096$ toward PKS 0405-123.[3] The system was identified previously by Bahcall et al. (1993) in Lyα absorption using the Faint Object Spectrograph on board *HST*. Aspects of this absorber have previously been discussed by Prochaska et al. (2004), Williger et al. (2006), Lehner et al. (2006), Tripp et al. (2008), and Thom & Chen (2008a,b) based on *FUSE* and *HST* observations. This absorber exhibits numerous metal-line absorption features in high-resolution spectra obtained using *FUSE* and STIS, as previously mentioned by Prochaska et al. (2004). The large spectral coverage of the combined *FUSE* and STIS spectra provides access to ~ 15 ions, including six oxygen ions (O^0 through O^{+5}), and the highly-ionized tracers of hot gas Ne VIII and Mg X. Coverage of the large number of ionization states of oxygen and other elements gives us the opportunity to study in detail the ionization mechanisms that may be at work in this gas and place constraints on the temperature of the absorbing material. This absorber is among the strongest 5% to 10% of all O VI systems, and the simulations predict strong absorbers like this are more likely to be associated with hot, collisionally-ionized material. The results of our analysis show that the $z \sim 0.495$ absorber toward PKS 0405-123 must contain a substantial photoionized component, and may or may not also contain $\gtrsim 2 \times 10^5$ K gas as part of a multiphase structure. The lack of significant Ne VIII and Mg X places limits on the amount of hot WHIM gas in this system.

We discuss out the observations used here in §2. In §3 we discuss our measurements of the properties of the absorber. We provide a detailed analysis of the possible ionization mechanisms in this system in §4, and we discuss the implications in §5. Finally, we summarize our principal results in §6.

2 OBSERVATIONS

In this work we present observations of the z= 0.495 absorber toward PKS 0405–123 taken by several UV spectrographs. Our analysis focuses on three spectroscopic datasets at UV wavelengths: (1) FUV spectra obtained with *FUSE* covering $\lambda \approx 912 - 1150$ Å ($R \approx 15000$); (2) STIS/E140M echelle spectroscopy acquired with *HST* covering $\lambda \approx 1150 - 1700$ Å ($R \approx 46000$); and (3) FOS/G190H spectroscopy from *HST* covering $\lambda \approx 1570 - 2330$ Å ($R \approx 1300$). We describe each of these datasets briefly below.

2.1 FOS Spectroscopy

PKS 0405–123 was observed with the FOS using the G190H grating and the C-2 ($0\farcs25 \times 2\farcs0$) aperture to feed the "blue" digicon as part of GTO program 1025 (PI: Bahcall). The total exposure time with the FOS was 3.8 ksec. These are pre-COSTAR data and have been described by Bahcall et al. (1993) and Jannuzi et al. (1998), among others. We adopt the reduced data from the uniform FOS reduction of Bechtold et al. (2002)[4] who describe their reductions in detail. We use the FOS data to study the Lyα absorption from the z= 0.495 absorber. This absorber is unresolved at the resolution of FOS ($R \approx 1300$ or $\Delta v \approx 230$ km s^{-1} FWHM). The data have a signal-to-noise ratio $S/N \approx 13$ per pixel, with four pixels per resolution element.

2.2 STIS Spectroscopy

PKS 0405–123 was observed by STIS using the E140M grating and the $0\farcs2 \times 0\farcs06$ aperture to feed the FUV MAMA detector as part of the GTO program 7576 (PI: Heap). This setup yields spectra with a velocity resolution $\Delta v \approx 7$ km s^{-1} (FWHM) with approximately two pixels per resolution element. The spectral coverage of the STIS data is $\lambda \approx 1150 - 1700$ Å. The total exposure time

[1] Verner et al. 1994b quote give wavelengths for the Mg X 624.950 Å and Si XII 520.665 Å transitions that are not in agreement with the wavelengths given in Verner, Barthel, & Tytler 1994a. The latter agree with those available via NIST. We quote the NIST wavelengths throughout for these transitions.

[2] The term multiphase will be used here to denote an absorber with a mixture of gas with differing temperatures and ionization states where these differences are often driven by differing ionization mechanisms.

[3] Hereafter we simply refer to this as the $z = 0.495$ absorber.

[4] The data are available through `http://lithops.as.arizona.edu/~jill/Quasar`

of the observations is 27.2 ksec. The data have $S/N \approx 5-7$ per pixel. The absolute velocities are accurate to $\sim 0.5-1.0$ pixels ($\sim 2-4$ km s^{-1}) while the relative wavelength scale is twice as good (Kim Quijano et al. 2003), though Tripp et al. (2005) have noted occasional wavelength scale errors in excess of these values.

The STIS data have been discussed extensively in the context of IGM absorption by Chen & Prochaska (2000) and Prochaska et al. (2004), who discuss metal line absorbers, as well as Williger et al. (2006) and Lehner et al. (2007), who concentrate on the properties of the H I absorption. Our reduction is that used by Lehner et al. (2007). Our measurements of the z= 0.495 system will differ slightly from Prochaska et al. given the slightly different reduction, our choice of integration limits, reconsideration of continuum placement, and other details.

2.3 FUSE Spectroscopy

PKS 0405–123 has been observed by *FUSE* (Moos et al. 2000; Sahnow et al. 2000) as part of GI programs B087 (PI: Prochaska) and D103 (PI: Howk) for a total exposure time of 142 ksec. Prochaska et al. (2004) and Chen & Prochaska (2000) have reported on aspects of the IGM; the data used here approximately double the exposure time of those earlier observations. The *FUSE* observations were taken in TTAG or photon event mode with the object centred in the LWRS ($30'' \times 30''$) apertures. The *FUSE* data have been uniformly reduced with CalFUSE v3.1 (Dixon et al. 2007). These data have a velocity resolution $\Delta v \sim 20$ km s^{-1} (FWHM) and are binned to 0.027 Å per pixel ($\approx 7-8$ km s^{-1} per pixel), giving roughly 3 pixels per resolution element. We have combined the data from all channels in regions of overlap to provide S/N~ 10 per pixel over the spectral range covered by the LiF channels ($\lambda \sim 1000-1180$ Å) and S/N~ 6 per pixel over the range covered by the SiC channels ($\lambda \sim 915-1000$ Å). While this coaddition of channels can lead to a slight degradation in the breadth and shape of the line spread function, the increase in S/N of data outweighs this slight effect.

The absolute wavelength calibration of *FUSE* is not well determined. We have set the zero point by comparing absorption lines from the Galactic interstellar medium in the *FUSE* bandpass with similar lines in the STIS bandpass, (e.g., comparing lines of Fe II, Si II, and O I between the instruments). This approach generally leads to zero-point uncertainties of order $\sim 2-5$ km s^{-1}, although our experience has shown this can occasionally be as large as 10 km s^{-1}.

3 THE $Z = 0.495$ ABSORPTION SYSTEM

The focus of this paper is the $z \approx 0.495$ absorption system toward PKS 0405–123 ($z_{em} = 0.574$). Here we discuss the velocity structure of the absorber and separately describe our analysis of the metals and H I in this system.

Figure 1 presents the normalized profiles of several important metal ions and Lyβ (see §3.2) in this absorber for an assumed zero point of $z = 0.495096$. The redshift is based on the centroid of the strong C III 977 Å transition. The continua were estimated by fitting low-order Legendre polynomials to regions free of absorption lines following Sembach & Savage (1992). Due to the simplicity of the quasar spectrum, most continua for this work were first order (linear) fits.

We identify significant metal line absorption in the C III 977 Å, N IV 765 Å, O IV 787 Å, O V 629 Å, and O VI 1031, 1037 Å transitions. The measurement of O V λ629 is the first direct detection of this ion in intervening absorbers at $z < 1$ (though see Telfer et al. 2002 for an indirect detection of the composite absorption from many Lyα forest clouds). In addition, our data include non-detections of strong lines from C II, N II, N III, O II, O III, Ne VIII, and Mg X, among others. We do not show profiles for all the ions covered by our data, as the upper limits for several are not particularly stringent or important in our final analysis.

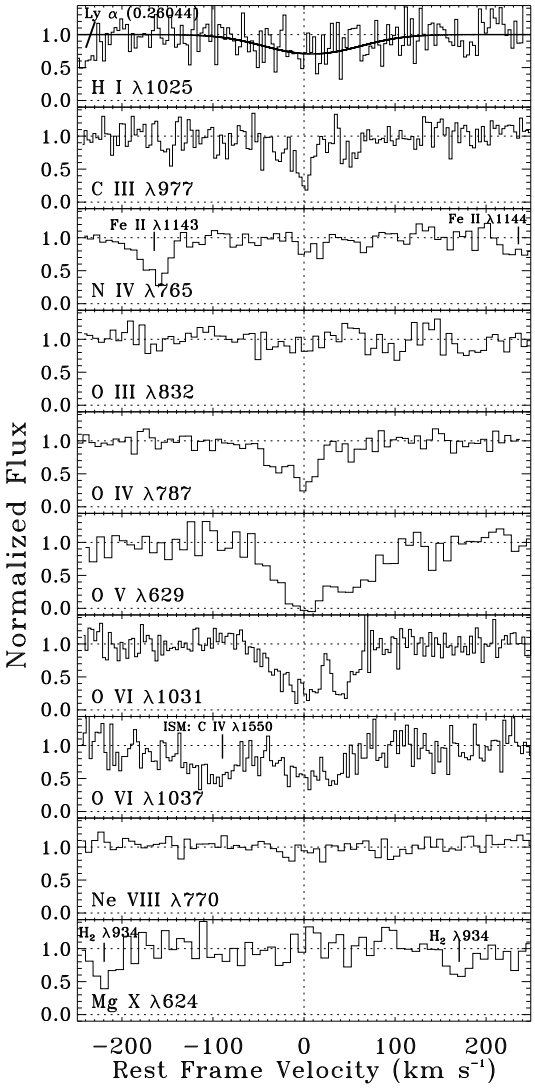

Figure 1. Absorption profiles the $z = 0.495096$ absorber toward PKS 0405–123 (the velocity zero-point was arbitrarily defined to match the central velocity of the main C III component derived through component fitting). These data, ordered by atomic mass and ionization state of the ions, are from *FUSE* ($\lambda_0 < 790$ Å) and STIS ($\lambda_0 > 790$ Å). The detection of O V is the first for intervening material at $z < 1$. The STIS data have a resolution of ≈ 7 km s^{-1} (FWHM) with two pixels per resolution element; the FUSE data have a resolution of ≈ 20 km s^{-1} with three pixels per resolution element.

3.1 Metal Ion Absorption

3.1.1 Apparent Column Densities and Velocity Profiles

Our measurements of the properties of the $z \approx 0.495$ absorbtion line system are presented in Table 1, including our assumed atomic data [taken from the compilations of Verner et al. (1994) and Morton (2003)]. The columns integrated over the profiles are given, derived using a combination of the apparent optical depth method (AOD) of Savage & Sembach (1991) and profile fitting techniques (described below). The apparent optical depth, τ_a of an absorption profile is written $\tau_a = -\ln[I(v)/I_c(v)]$, where $I(v)$ and $I_c(v)$ are the observed intensity across the profile and the estimated continuum intensity, respectively. The apparent column density, $N_a(v)$, is then $N_a(v) = [(m_e c)\tau_a(v)]/[(\pi e^2)(f\lambda)]$. In the absence of unresolved saturation, the apparent column density is a valid, instrumentally blurred representation of the true column density distribution. Those regions of the profile exhibiting unresolved saturated structure will be lower limits to the true column density. The integration of the $N_a(v)$ profile is the total apparent column density, which is reported in Table 1, along with the equivalent widths of the absorption. All of the upper limits given here are 3σ following Wakker et al. (1996). The O VI absorption deserves some discussion, which we postpone to §3.1.3. We have given values for C III and O IV derived from profile fits to the data for these ions (see below). The $N_a(v)$ integrations, which are not as reliable as the profile fits for these ions, give $\log N(\text{C III}) > 13.31$ and $\log N(\text{O IV}) > 14.38$.

We show the $N_a(v)$ profiles of several ions in Figure 2. With Figure 1, these figures show the gas in this system can be broken into three main absorption blends centred at $v \sim -30, 0$, and $+50$ km s^{-1}, which we refer to as components 1, 2, and 3, respectively. These components are most prominently viewed in the profiles for C III, O IV, and O V.

3.1.2 Profile Fitting of Metal Lines

The O IV and C III profiles show quite strong absorption in the central component 2 ($v \sim 0$ km s^{-1}), with peak apparent optical depths of $\tau_a \approx 1.4$ and 1.7, respectively. Such large apparent optical depths suggest there may be some unresolved saturated structure in the profiles, making the measured apparent column densities lower limits to the true columns. An alternate way to derive the column densities is to fit an instrumentally-smoothed model to the absorption profiles of these species. We use the profile fitting software of Fitzpatrick & Spitzer (1997) for this purpose. The parameters for the fit are the central velocity, Doppler parameter (*b*-value), and column density of each assumed component or cloud. The approach assumes each component can be described by a Maxwellian velocity distribution.

The fits depend on the adoption of an instrumental line spread function (LSF). For the STIS observations of C III λ977, we adopt the STIS E140M LSF from Kim Quijano et al. (2003). For the FUSE observations of O IV λ787 we adopt a Gaussian LSF with a FWHM of 20 km s^{-1}. The true breadth and shape of the FUSE LSF are uncertain (see below).

The C III and O IV profiles were both well fit by a three component model, mirroring our discussion of the component structure above, with reduced χ^2 values very near unity. The precise χ^2 values are sensitive to the range over which they are calculated, mostly driven by the presence of large noise excursions (e.g., near $v \sim -47$ km s^{-1} in the C III profile; see Figure 1). The results of the profile fitting for these transitions, which we fit independently, are given in Table 2. Comparing the total columns derived in this way with the $N_a(v)$ integrations (see previous subsection) suggests significant corrections to the apparent columns due to saturation effects are required. Figure 3 shows the component models for each fit with the original data.

The O IV results are derived from a fit of the *FUSE* data. This

Table 1. Integrated Equivalent Widths and Column Densities[a]

Ion	IP [eV][b]	λ_0 [Å]	f[c]	W_r [mÅ]	$\log N_a$
H I	0 – 13.6	1215.670	0.4162	540 ± 80	14.07 ± 0.06[d]
H I	0 – 13.6	1025.722	0.0791	90 ± 19	14.22 ± 0.09[d]
H I	0 – 13.6	972.537	0.0290	< 50	< 14.31[c]
C II	11.3 – 24.4	903.962	0.336	< 32	< 13.12
C III	24.4 – 47.9	977.020	0.757	89 ± 9	13.39 ± 0.05[e]
N II	14.5 – 29.6	1083.990	0.111	< 54	< 13.68
N III	29.6 – 47.4	989.799	0.123	< 38	< 13.55
N IV	47.4 – 77.5	765.148	0.616	29 ± 9	$13.01^{+0.11}_{-0.16}$
O II	13.6 – 35.1	834.465	0.132	< 40	< 13.68
O III	35.1 – 54.9	832.927	0.107	< 36	< 13.73
O IV	54.9 – 77.4	787.711	0.111	106 ± 8	$\gtrsim 14.37$[f]
O V	77.4 – 113.9	629.730	0.515	218 ± 8	> 14.39
O VI	113.9 – 138.1	1031.926	0.1325	215 ± 9	14.47 ± 0.02[g]
O VI	113.9 – 138.1	1037.617	0.0658	95 ± 13	14.50 ± 0.05[g]
Ne VIII	207.3 – 239.1	770.409	0.1030	< 29	< 13.73
Ne VIII	207.3 – 239.1	780.324	0.0505	< 25	< 13.97
Mg X	367.5 – 367.5	624.950	0.041	< 44	< 14.49
S VI	72.6 – 88.1	933.378	0.437	< 23	< 12.83

Note: a: All upper limits are 3σ. Ions with rest wavelengths $\lambda_0 > 880$ Å are from STIS observations, with $\lambda_0 < 880$ from *FUSE* observations. *b*: The range of creation and ionization energies for each species (Däppen 2000). *c*: Atomic oscillator strengths from Morton (2003) for $\lambda_0 > 912$ Å and Verner et al. (1994) for $\lambda_0 < 912$ Å. *d*: We adopt a total H I column density of $\log N(\text{H I}) = 14.29 \pm 0.10$ based on a combined profile fitting analysis of the three transitions reported in this table. The integrations here cover the entire breadth of the profile. *e*: Adopted from a component-fitting analysis. *f*: Column density lower limit from a straight integration of the apparent column density. A component-fitting analysis gives 14.50 ± 0.08, but it is sensitive to the assumed properties of the FUSE LSF. See text. *g*: We adopt a total O VI column density of $\log N(\text{O VI}) = 14.47 \pm 0.02$ based on a weighted mean of the two lines, including absorption from the discrepant areas. The amount of O VI associated with components 1, 2, and 3, is $\log N(\text{O VI}) = 14.41 \pm 0.05$ (see §3.1.3). This is the value used in our modeling.

Table 2. Component Fitting Results

Ion	Component	v_c [km/s][a]	$\log N$	b [km/s]
C III	1	-26.7 ± 1.8	12.56 ± 0.15	... [d]
	2	0.0 ± 1.0[b]	13.20 ± 0.06	8.5 ± 1.5
	3	$+50.7 \pm 2.1$	12.70 ± 0.10	8.9 ± 3.8
O IV	1	-33.3 ± 2.1	13.90 ± 0.08	7.8 ± 5.6
	2	$+1.5 \pm 1.3$	14.31 ± 0.11[c]	9.1 ± 2.9
	3	$+51 \pm 3$	13.47 ± 0.11	... [d]

Note: a: Central velocity relative to $z = 0.495096$. *b*: Our adopted redshift is defined by the central velocity of this component. *c*: Given the low resolution of *FUSE* and the behavior of the profile fitting for this component, the quoted column density should be considered a lower limit. *d*: The *b*-value of this component is held fixed in the fitting to avoid fitting an unreasonably-low value. The absorption is weak enough that the column density is not very sensitive to the adopted *b*-value.

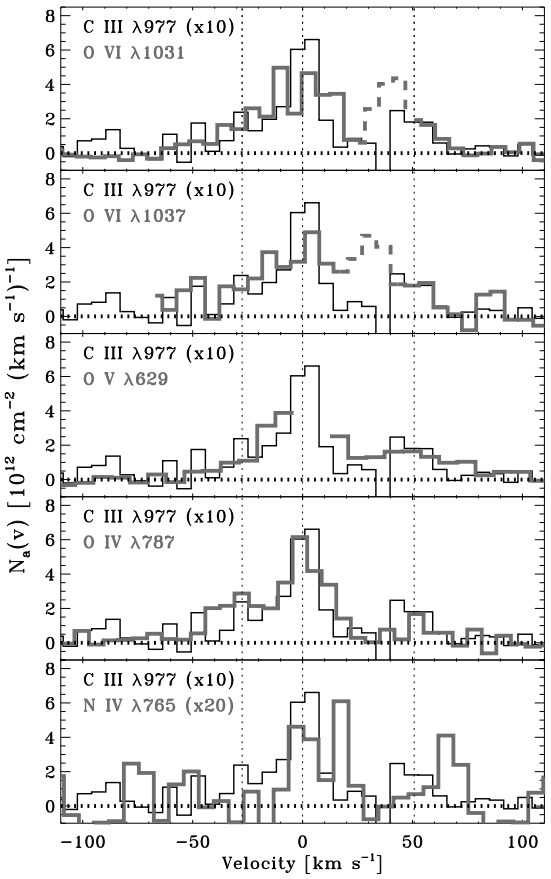

Figure 2. Apparent column density profiles of metal ions in the $z = 0.495096$ absorber toward PKS 0405–123. Both O VI lines are shown given the differences between them (see §3.1.3), which is shown by the dashed regions. The profile for C III is shown in each panel, multiplied by a factor of 10 to match the scale of the other ions. There is good agreement in the component structure between most of the ions. The thin dashed vertical lines show the locations of the components fit to the C III profile (see §3.1.2 and Figure 3). The STIS observations (transitions with $\lambda_0 > 790$ Å) are binned by a factor of two to approximately one datum per resolution element (~ 7 km s^{-1}). The FUSE data have approximately the same pixel spacing, with three pixels per 20 km s^{-1} resolution element.

line is observed both by *FUSE* and STIS, although the STIS data have very low S/N (see, e.g., Williger et al. 2006). We have tested the effects of simultaneously fitting the *FUSE* and STIS data and find no differences in the results. This is not surprising: because the fits are weighted by the variance of the data, the low S/N of the STIS data insures they do not contribute to the fits nearly as much as the *FUSE* data. However, the column density of O IV can be sensitive to the adopted width of the *FUSE* LSF, whose shape is poorly-constrained, due to the change in the fitted b-value. Furthermore, additional components in the O IV profile can cause significant increases in the column density and are not well constrained on the whole. A $\pm 10\%$ change in the FWHM of the assumed LSF leads to

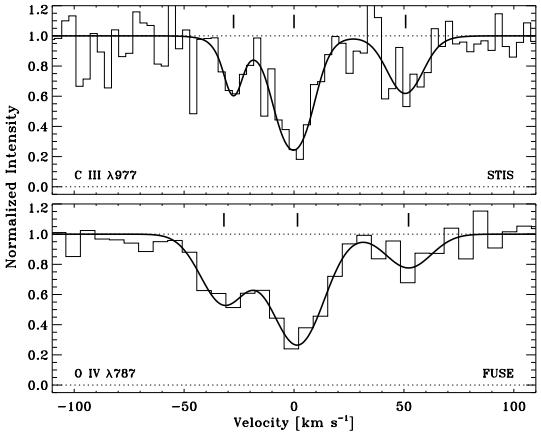

Figure 3. The normalized absorption profiles of C III λ977 and O IV λ787 with the adopted profile fits overlayed, assuming a redshift of $z = 0.495096$. The properties of the three components used in these fits are summarized in Table 2. The velocity centroids are shown by thick black ticks above each spectrum. See the text for details of the fitting procedure.

changes in the total O IV column of -0.06 and $+0.10$ dex. As the LSF breadth is increased, the errors in the determination become quite large due to the increasing dependence on the b-value with increasing saturation of the model. (For an LSF with FWHM≈ 22 km s^{-1}, the uncertainties are nearly an order of magnitude.) Given these uncertainties, we will proceed by adopting the lower limit to the O IV column from the $N_a(v)$ integration discussed above.

The STIS observations of C III have significantly higher resolution and a well understood LSF. The contribution from extra components is much more stringent for the C III profile, as they do not affect the column density without increasing the χ^2 value significantly and/or requiring unphysical b-values (e.g., $\approx 1-2$ km s^{-1}, implying temperatures too low for the IGM) for the additional components. We feel that the column densities and errors derived from our profile fitting analysis of the C III profile are good measures of the true column. In what follows we adopt the profile fitting results for C III, as noted in Table 1.

3.1.3 The O VI Absorption

The $N_a(v)$ profiles of the weak and strong transitions of O VI at 1031.926 Å and 1037.617 Å, respectively, are shown in Figure 4. For velocities $v \lesssim +20$ km s^{-1} these transitions are in good agreement. However, they do not agree with one another or the other metal ions at larger positive velocities (see Figure 2). A quick glance at Figures 1 and 4 reveals what appears to be a return to the continuum in the strong line that is not present in the weak line. Examining the $N_a(v)$ profiles in Figure 4, the peak of column density distribution at velocities $v > +20$ km s^{-1} occurs at different velocities in the two profiles. The "component" seen at $v \approx +30$ to $+40$ km s^{-1} in Figures 2 and 4 is not observed in other ions save perhaps O V. However, one does see component 3, at $v \approx +50$ km s^{-1} as seen in other metal ion profiles, in both profiles. This can be seen in Figure 2 (comparing, for example, the two O VI profiles with O IV or C III).

The difference between the two members of the doublet could be due to contamination of *both* profiles by intervening Lyα absorption with peak optical depths that yield consistant $N_a(v)$ inte-

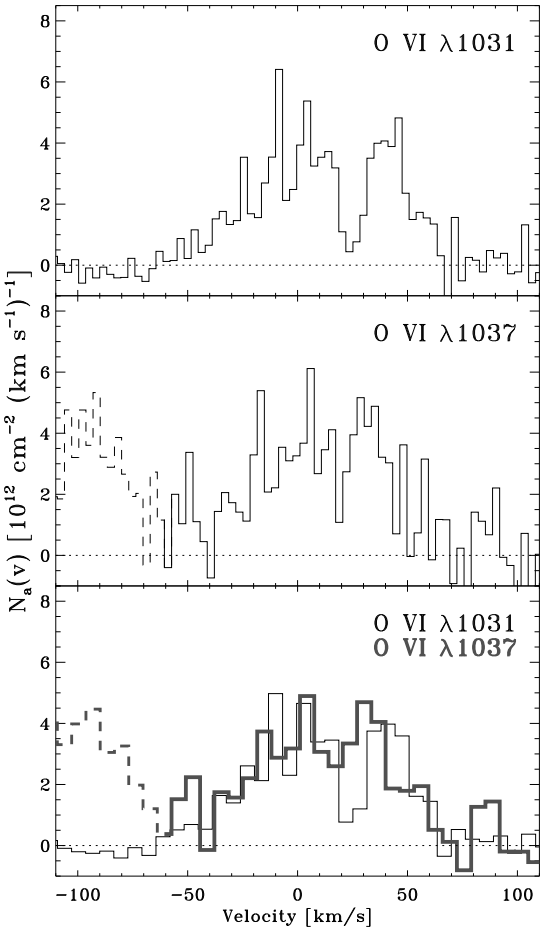

Figure 4. Apparent column density profiles of the O VI transition from the $z = 0.495096$ absorber toward PKS 0405–123. The top two panels show the strong and weak lines, at 1031.926 and 1037.617 Å, respectively, at full sampling. The bottom panel shows both $N_a(v)$ profiles binned by two pixels (to one pixel per resolution element). At velocities $15 \lesssim v \lesssim 45$ km s^{-1}, the discrepancies in the two profiles are caused by intervening transitions, presumably Lyα.

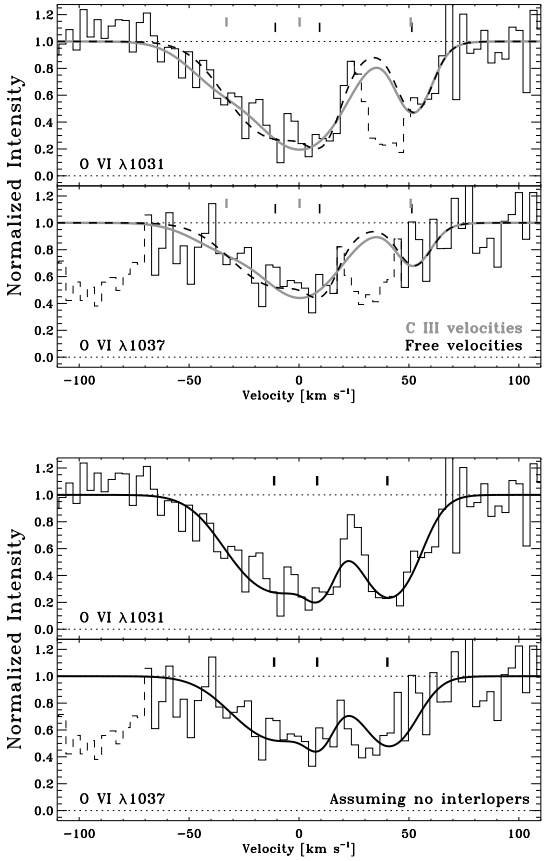

Figure 5. The normalized absorption profiles of O VI λλ1031 and 1037 with profile fits overlayed. The top two panels show the profiles assuming the O VI lines are contaminated with interloping absorbers (thin dashed lines denote regions of the data we assume to be contaminated). Two fits are shown in these panels: one assuming a three component fit with velocities fixed to those found in C III and the other allowing the velocities of the O VI components to be a free parameter. The reduced χ^2 values are indistinguishable for these two models. The bottom two panels show our fits assuming there is no contamination of the profiles. The χ^2 is significantly worse in this case. (However, the contribution to the χ^2 values for the range of data assumed to be contaminated in the upper panels is minimized by artificially increasing the variance of the data over those ranges.) The total column density for the models in the upper panels are both consistent with $\log N(\mathrm{O\ VI}) = 14.40$ (albeit with much different errors; see text) whereas the bottom panels give $\log N(\mathrm{O\ VI}) = 14.50 \pm 0.13$. The discrepancy is due to the lower equivalent width attributed to O VI in the upper panels.

grations if one assumes they are O VI. Limits on Lyβ absorption at the appropriate redshifts do not rule this out. Alternatively, as noted by Tripp et al. (2008), this misalignment could be due to small scale errors in the STIS geometric distortion correction, as have been identified, e.g., by Jenkins & Tripp (2001). Such difficulties are neither well characterized for STIS nor common.

While "hot pixels" can create discrepancies like those seen here (see discussion in Tripp et al. 2008), the observations of PKS 0405–123 were taken in two visits with the echelle orders displaced signficantly between the visits. The data extracted for the two visits individually are consistent over these wavelength regions, which would not be the case for hot pixels fixed on the detector. Thus, this explanation is not tenable.

We have attempted to simultaneously fit the profiles of the O VI doublet as observed by STIS. Aside from the velocity range of possible contamination, the $N_a(v)$ profiles of the 1031 and 1037 Å transitions seen in Figure 4 are in good agreement, implying the effects of unresolved saturation cannot be large (as also evidenced by the agreement in integrated apparent columns, see Table 1). The fitting was undertaken to attempt to disentangle the component structure of the absorption and to provide a measure of the column density of the higher velocity components, especially component 3 ($v \approx +50$ km s^{-1}), which is strongly blended with the contaminated or compromised regions. We attempted fits under two assumptions: 1) the discrepant regions in the O VI lines are contaminated by interloping absorbers; and 2) the discrepant regions suffer from difficulties in the wavelength assignment, but represent O VI absorption associated with this absorber.

In the first of these fits, we artificially increased the variance over the velocity ranges $+23 \leqslant v \leqslant +53$ km s^{-1} and $+19 \leqslant v \leqslant +43$ km s^{-1} for the 1031 and 1037 Å transitions, respectively, to such large values that they do not affect the calculation of χ^2 and, hence, the parameters of the fit. The fits to the regions encompassed by components 1 and 2 are non-unique, and

can be fit with one, two, or three components with similar values of χ^2. Part of the difficulty in fitting these lower-velocity components is the loss of information on the positive velocity side of the profiles due to the assumed contaminating absorption. In addition, the component structure in the O VI profiles is not distinct. This is in contrast to the C III and O IV profiles in this region. If the component structure is assumed to follow that of C III, with velocities fixed to those in Table 2, the total column density for this model is $\log N(\mathrm{O\ VI}) = 14.41 \pm 0.05$. The fit is shown in Figure 5 as the thick grey line, with the central velocities of the components shown above the profiles. A fit in which velocities of the O VI components to be a free parameter is also shown as the thick dashed black line (the black ticks above the profiles show the central velocities in this case). The total column density is $\log N(\mathrm{O\ VI}) = 14.40 \pm 0.16$. In this fit, the largest column density is in component 1; the large fitted b-value for this component has a significant uncertainty, which is the source of the much larger error in this model than that with the velocities fixed to the C III solution. Both fits have indistinguishable values of χ^2. In each case the columns of component 3 are very nearly the same near $\log N(\mathrm{O\ VI})_3 = 13.63 \pm 0.14$ (the value if the velocity is allowed to vary).

The second fit, which assumes all of the absorption is O VI associated with this system, is shown in the bottom two panels of Figure 5. These plots show the nature of the difficulty quite well for the positive velocity component. Components 1 and 2 are virtually indistinguishable from the fits above where the velocities are allowed to vary. The total column density in the O VI fit is $\log N(\mathrm{O\ VI}) = 14.50 \pm 0.13$, some $+0.1$ dex higher than that derived above. We somewhat favor this total column over the lower value. The total equivalent width for the full profile is $W_r(\lambda 1031\ \text{Å}) = 215 \pm 9$ mÅ (see Table 1), which places this absorber in the top 10% of the ≈ 50 intervening O VI absorbers studied in the recent survey of Tripp et al. (2008). The column and equivalent width values in this assumption are consistent with those derived by Tripp et al. (2008) and Thom & Chen (2008b).

We focus our ionization analysis on the gas associated with components 1, 2, and 3, excluding the additional column over the discrepant region in O VI that does not appear in C III and O IV. Because the discrepant component is not seen in C III or O IV, it must have significantly different ionization conditions than the rest of the gas, and we do not attempt to model it. Because most of our models will assume a solar C/O ratio, metallicities [C/H] derived from C III will also imply a given [O/H]. Thus for our ionization and metallicity calculations (when they depend on O VI) will adopt the fit fixed to the C III velocities, which gives $\log N(\mathrm{O\ VI}) = 14.41 \pm 0.05$. This excludes a component at $v \approx +40$ km s^{-1}, but includes absorption from component 3 at $v \approx +50$ km s^{-1} (top panels in Figure 5).

This value is preferred over that in which the velocities of the O VI are allowed to freely float because the uncertainties become unreasonably large in the latter case in our estimation. An integration of the $N_a(v)$ profile of O VI over the uncontaminated region at $v \lesssim +20$ km s^{-1} yields $\log N(\mathrm{O\ VI}) = 14.30 \pm 0.05$ (a mean of the two O VI lines). Adding the column associated with component 3 from above, this gives a total column density of $\log N(\mathrm{O\ VI}) = 14.38 \pm 0.05$ excluding the compromised regions (i.e., for components 1 to 3). Thus, the uncertainty derived using a model with velocities fixed to those found in C III provides an uncertainty closer to the $N_a(v)$-derived values. We note that including absorption associated with component 3 only impacts the metallicities – the ratios of O VI/C III and O IV/C III derived for components 1 and 2 are consistent with the ratio after including component 3, which adds $\sim +0.1$ dex to these three ions. Thus, had we chosen to model the clearly-uncompromised velocity range, we would derive the same results as those presented below.

3.1.4 Limits on the Multiphase Structure from Velocity Profiles

The $N_a(v)$ profiles shown in Figure 2 demonstrate that the ions C III, O IV, O V, and O VI in this absorber have a similar velocity structure, with gas associated with the three components discussed above (and perhaps a fourth seen in O VI and O V). The profile fitting results of §3.1.2 reinforce this basic structure, though with the caveat that the limited resolution of the data could be hiding substructure within the components (or component blends) identified in Table 2. The H I and metal ions would be considered "well-aligned" in the categorization of Tripp et al. (2008) since their central velocities are consistent with one another within 2σ. However, the uncertainties in the H I centroid are relatively large, so the meaning of this alignment is not clear. In addition, too little information is available for Lyman-series absorption to know if the detailed component structure hinted at in the metal ions is mirrored in H I.

While the metal line profiles in Figure 2 are generally similar, there are hints of differences between them. The broad envelope of the O VI distribution (at $v \lesssim +20$ km s^{-1}) is similar to the O IV and C III distributions, and the total velocity extents of O VI, O IV, and C III are all very similar (including the gas in component 3 at $v \approx +50$ km s^{-1}). However, O VI seems less prominent over the velocity range of component 2 compared with the lower-ionization species. This may be due to changing ionization conditions between components 1 and 2, with a corresponding change in the ionic ratios, or due to somewhat broader components in O VI. These differences, however, are at the limits of the noise and resolution of the current data. It is difficult to say whether or not they are significant. If so, they may imply the existence of a warmer phase of the gas traced by O VI and a cooler phase traced by C III and O IV. However, if this is true, *both phases must be present at the same velocities*.

The component Doppler parameters given in Table 2 limit the temperature of the gas. For example, the b-values of C III and O IV for component 2 imply maximum temperatures of $T \lesssim (5.2 \pm 1.8) \times 10^4$ K and $\lesssim (8 \pm 5) \times 10^4$ K, respectively. [5] The contribution of a hot component to these species must not produce absorption profiles broader than observed. To test whether a significant amount of warm-hot gas (with $T > 10^5$ K) could be included in these profiles, we have fit the C III and O IV profiles including an additional component forced to have a b-value appropriate for gas with $T \gtrsim 10^5$ K. For C III, we find that any broad components added in this way must have negligible column densities in order to be consistent with the observed profiles. This is not unexpected given the small ionization fraction of C III in gas with such temperatures (see below). For O IV, one can include a broader component centred near ≈ 0 km s^{-1}. Adopting a b-value of 10 km s^{-1}, corresponding to $T \lesssim 10^5$ K for such a component leads to very small column densities in that component or forces the existing component 2 to have unphysically-low b-values (implying temperatures much lower than expected for the IGM) for reasonable values of χ^2. If one assumes $b = 16$ km s^{-1}, corresponding to $T \lesssim 2.5 \times 10^5$

[5] The profile fits O IV are uncertain as discussed above. Lowering the FWHM of the assumed LSF for FUSE to 18 km s^{-1} allows for temperatures $\lesssim (1.0 \pm 0.5) \times 10^6$ K.

K, the fits are significantly better. Our fits suggest at most 30% of the total column of O IV can come from such a component. This limit comes about because as the column of the broad component is increased above $\log N(\mathrm{O\ IV}) \approx 13.7$, the column of the existing component 2 increases as well (due to a decreasing b-value for component 2). This conclusion is robust to changes in the adopted LSF for FUSE. It is mostly driven by the nature of a multicomponent curve of growth, where the b-value of the narrow component is decreased in order to account for an increased contribution to the equivalent width from the broad component. The decrease in the b-value for the narrow component increases the total column density substantially, always keeping the broad component to $\lesssim 30\%$ of the total.

Thus, given the profile comparisons and the profile fitting results, there may be room, if not some evidence, for a multiphase structure within this absorber. The discrepancies between the $N_a(v)$ profiles of the ions that might imply a multiphase structure are subtle compared with those seen in many absorbers (e.g., Tripp et al. 2008), and the O VI and other ions are reasonably well aligned with the H I in this system (see Figure 1). If broad, warm-hot ($T \gtrsim 10^5$ K) gas is present, it can only contribute $\lesssim 30\%$ of the total column of O IV and must have a negligible contribution to the C III column density. In such a scenario, O VI may preferentially trace the warm-hot material, C III would trace the cooler gas (at $T \lesssim 5 \times 10^4$ K), and O IV would include contributions from both, albeit with a larger contribution from the cooler matter. The warm-hot gas traced by O VI in such a scenario cannot be too hot ($T \lesssim 3 \times 10^5$ K) in order to avoid producing too much Ne VIII or too little O V (see §4).

3.2 H I Lyman-series Absorption

Figure 6 shows the normalized absorption line profiles from the Lyα, Lyβ, and Lyγ transitions of neutral hydrogen for the $z = 0.495$ absorber. The Lyα observations are taken from the low-resolution FOS data (≈ 230 km s^{-1} FWHM), while the Lyβ and Lyγ are from the high-resolution STIS data (≈ 7 km s^{-1} FWHM). The Lyα transition is poorly resolved by the FOS, the Lyβ line is poorly detected by STIS, and Lyγ is undetected. We, therefore, have very little information on the velocity structure of the H I in this system.

Table 1 reports our integrated restframe equivalent widths and limits for these transitions. The Lyα line integration is over the range ± 350 km s^{-1}, while the integration for Lyβ and Lyγ is over ± 85 km s^{-1}. To better constrain the H I column in the face of the resolution and detection limitations, we have performed a simultaneous profile fit to these three transitions as described above (see also Appendix in Lehner et al. 2007 for this absorber). We adopt a Gaussian line spread function (LSF) for the FOS data and allow for a shift in the FOS data relative to the STIS data given the better absolute wavelength calibration of the latter.

The results of the fit are shown in Figure 6 as the smooth solid lines. We note that the results of the fit are somewhat sensitive to the range over which one calculates the χ^2 goodness of fit parameter. We have investigated the range of column densities implied as one varies these limits, incorporating an estimate of this variability into our error estimate. From this analysis, we adopt a best-fit column density of $\log N(\mathrm{H\ I}) = 14.29 \pm 0.10$. This yields a b-value of $b = 68 \pm 8$ km s^{-1} for a single component fit to the profiles with a central velocity of $v_c = +9 \pm 8$ km s^{-1} relative to $z = 0.495096$ (from C III).

Our adopted H I column is comparable to the values derived from earlier studies that include this absorber: $\log N(\mathrm{H\ I}) = 14.31 \pm 0.07$ (Tripp et al. 2008), 14.3 ± 0.1 (Thom & Cen 2008b), 14.39 ± 0.07 (Williger et al. 2006), and > 13.95 (Bahcall et al. 1993, using their Lyα equivalent width). The central velocity is driven by the Lyβ detection shown in Figure 6; obviously there is significant uncertainty in this determination given the poor quality of that profile. While the derived velocity is within $\sim 1\sigma$ of the central value of C III, O VI and other ions, the poor quality of the H I determination limits our ability to draw significant conclusions from this alignment. As discussed above, the H I would be described as "well-aligned" under the Tripp et al. (2008) definition since the central velocities of H I and O VI are within 2σ of one another. The b-value provides a firm limit to the weighted mean temperature of the H I-bearing gas of $T \lesssim (2.8 \pm 0.7) \times 10^5$ K assuming pure thermal broadening. The b-value assumes a single component describes the H I broadening, though our data are not of high enough quality to determine if the H I component structure follows that of the metals (with multiple components).

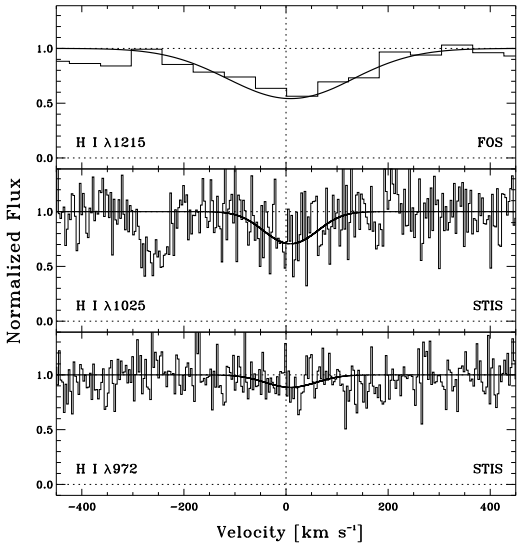

Figure 6. Absorption profiles of the H I Lyα, Lyβ, and Lyγ transitions associated with the $z = 0.495096$ absorber toward PKS 0405–123 (the velocity zero-point was defined by the peak of the C III absorption). The Lyα absorption is from the low-resolution FOS spectrum, while the other two are from the high resolution STIS data. The histograms show the data, while the smooth solid lines show a simultaneous profile fit to the three lines (see §3.2).

4 IONIZATION OF THE ABSORBER

Given the importance of O VI as a tracer of shock-heated gas in the low-redshift IGM, the presence of strong O VI in the $z = 0.495$ absorber toward PKS 0405–123 might imply this system is tracing the WHIM at low-redshift. However, as emphasized by a number of authors (Tripp et al. 2008, Thom & Chen 2008b, Lehner et al. 2006, Prochaska et al. 2004, Savage et al. 2002), O VI may not be a pure tracer of shock-heated WHIM material. If not associated with the WHIM at $T > 10^5$ K, it may trace cooler shock-heated gas, the metal-enriched Lyα forest, or photoionized regions in the extended halos of galaxies.

There are two principal mechanisms for the ionization of the

gas being considered here: photoionization by the UV background and collisional ionization. The characteristics of photoionized gas depend on the shape and strength of the ionizing spectrum and on the density of the gas, while the properties of collisionally ionized gas depend principally on the temperature of the gas. Gas that is predominantly photoionized will have characteristic temperatures of order a few times 10^4 K. Collisional ionization models of IGM absorbers are usually constructed to explain highly ionized gas and adopt temperatures $\sim 10^5$ K and above (e.g., Gnat & Sternberg 2007, Cen et al. 2006), although lower temperatures are affected by collisions as well.

The presence of strong O VI in the absorber being studied here may arise due to the photoionization of a low density absorber, to the presence of hot gas or gas that has cooled from high temperatures in a non-equilibrium manner, or from a mixture of these. In this section we consider pure photoionization and pure collisional ionization models for the gas making up this absorber, showing that neither type of model fits the data sufficiently well. We also investigate an admixture of photoionized and collisionally ionized material, a scenario with some support from the comparison of the O VI and C III or O IV velocity structure.

Though there are likely regimes in which either photoionization or collisional dominates, IGM gas will have contributions from both of these mechanisms: photons will be present in intergalactic space and collisional ionization is important for at least hydrogen above $\sim 10^4$ K. Sophisticated models that account for the impact of both are beyond the scope of this paper (see Wiersma, Schaye, & Smith 2008, Cen & Fang 2006 for recent attempts at such models within large scale simulations). We consider a small number of models in which high temperature gas is exposed to ionizing photons, though ours is not an extensive exploration of that approach.

We assume that the observed H I and metal ions in this absorber are nearly cospatial and that the absorber has uniform abundances. We use solar relative abundances as a starting point for comparing ions of C, N, O, Ne, and Mg to models. Unfortunately, there is some controversy about the relative abundances of these elements in the solar system. Meteoritic abundances of Mg are well-determined and give a good abundance measure for the solar system (with the Mg to Si abundance in meteorites being referenced to the photospheric Si abundance to provide an absolute Mg abundance); we adopt $\log \mathrm{Mg/H} = -4.46$ (Lodders et al. 2009). The abundance of Ne is typically measured relative to O in the corona, and we assume Ne/O$= 0.15$ or $\log \mathrm{Ne/O} = -0.82$ (e.g., Asplund, Grevesse, & Sauval 2005a, Basu & Antia 2008).

Solar system abundance estimates for C, N, and O depend on photospheric abundances (see recent overviews by Lodders et al. 2009, Asplund et al. 2005a, and Lodders 2003). Recent adoption of 3D hydrodynamic models in analyzing the photospheric data have led to significantly lower abundances (see Asplund 2005) than earlier results (e.g., Anders & Grevesse 1989). This is particularly true for O, for which Asplund et al. (2004) derive $\log \mathrm{O/H} = -3.34 \pm 0.05$ compared with the earlier standard of $\log \mathrm{O/H} = -3.17 \pm 0.06$ (e.g., Grevesse & Sauval 1998). Such a low abundance causes significant difficulties with helioseismology models (e.g., Bahcall et al. 2005, Basu & Antia 2008), and there are arguments in favor of the higher abundances (e.g., Ayres 2008, Delahaye & Pinsonneault 2006, and others).

We will proceed by following the recent critical summary of abundances by Lodders et al. (2009) and assume $\log \mathrm{O/H} = -3.27 \pm 0.07$ (an average of values from Caffau et al. 2008, Ludwig & Steffen 2008, and Melendez & Asplund 2008). With our adopted solar system Ne/O ratio, this implies $\log \mathrm{Ne/H} = -4.09$.

The abundance of C advocated by Lodders et al., $\log \mathrm{C/H} = -3.61 \pm 0.04$ (an average of results from Allende-Prieto et al. 2002, Asplund et al. 2005b, and Scott et al. 2006) is less controversial. Lodders et al. recommend $\log \mathrm{N/H} = -4.14 \pm 0.12$ from Caffau et al. (2009); though this result has not yet appeared in press we adopt this value for consistency. For comparison, Asplund et al. (2005a) advocate $\log \mathrm{N/H} = -4.22 \pm 0.06$. For Mg we adopt $\log \mathrm{Mg/H} = -4.46 \pm 0.06$ (Lodders et al. 2009).

4.1 Collisional Ionization Models

Ionization of metals by collisions (primarily with electrons) can lead to high-stage metal ions if the gas temperature is sufficiently high. This is what drives the WHIM models, in which the high temperatures are a result of high velocity shocks as gas accretes onto filaments, groups, and clusters of galaxies (e.g., Cen & Ostriker 1999, Davé et al. 1999, Furlanetto et al. 2004, Kang et al. 2005, Bertone et al. 2008). These works emphasize the potential importance of O VI for tracing this material, though several cosmological simulations also predict that some of the O VI likely traces cool, photoionized gas (e.g., Cen et al. 2001, Fang & Bryan 2001, Chen et al. 2003, Kang et al. 2005, Oppenheimer & Davé 2009).

Given the strong O VI in the absorber studied here, it is worth considering if the ionization of the absorber can be explained primarily through collisional ionization. We use the recent models of Gnat & Sternberg (2007) to test whether collisional ionization can explain the relative distribution of ionization states in the $z = 0.495$ absorber toward PKS 0405–123. These authors have calculated new collisional ionization calculations with up-to-date atomic physics. They discuss models under the assumption of collisional ionization equilibrium (CIE) as well as non-equilibrium (NEQ) cooling models in which gas initially at $T = 5 \times 10^6$ K cools isochorically or isobarically.

One may argue against single-temperature CIE models for this absorber without detailed calculations, as the profile fits to the C III profiles suggest temperatures well below the $T \gtrsim 10^5$ K needed to produce significant O VI absorption in CIE. A comparison of the ionic ratios for the species in Table 1 shows no single temperature for which all of the data can be matched by the CIE models. This is demonstrated in Figure 7, which shows the column density ratios predicted by the Gnat & Sternberg CIE models for a number of species, identifying temperatures over which the models are consistent with the data for each of the ratios. The difficulties are principally in simultaneously matching the ratios of C III to O VI and limits on O III to C III. Prochaska et al. (2004) and others have emphasized that C III and O VI cannot coexist in significant amounts in single-temperature CIE models. The temperature limits derived for the C III in this absorber provide support for this conclusion.

The column densities may be better matched if one assumes a two-temperature structure for the absorber, with both phases in CIE. In this ad hoc model, one assumes that the O VI traces a warm-hot phase and that the C III traces a separate warm phase, perhaps a low-temperature WHIM like that discussed by Kang et al. (2005). The upper and lower panels of Figure 7 show the constraints for each of the independent temperature regimes. The temperature of the O VI-bearing medium is constrained to be in the range $2.3 \times 10^5 \lesssim T \lesssim 4.7 \times 10^5$ K by the upper limits for O III and Ne VIII at the low and high end of the range, respectively. In this case the C III-bearing gas, if in CIE, would itself require $T \lesssim 10^5$ K based on the O III to C III ratio, consistent with the C III b-values. In this scenario, O IV and O V are present in both temperature regimes, though most of these ions must reside in the

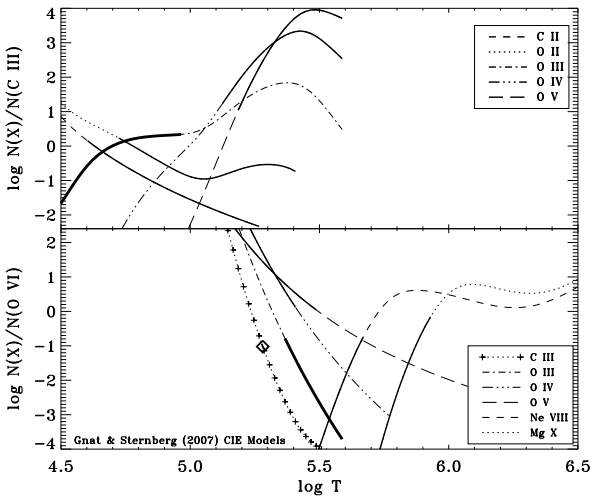

Figure 7. Column density ratios of several ions relative to C III (*top*) and O VI (*bottom*) as a function of temperature for the CIE models of Gnat & Sternberg (2007). The solid lines represent regions for which each of the ratios is consistent with the observations of the $z \approx 0.495$ absorber toward PKS 0405–123. Note that the O III/C III and O III/O VI ratios cannot be simultaneously matched for any temperatures. Furthermore, the C III/O VI ratio is not matched for temperatures consistent with the line width of the C III. (The narrow range of temperatures for which C III/O VI is matched is denoted by the diamond in the bottom panel.) The full range of temperatures is not shown in each panel because of the limited range of temperatures over which Gnat & Sternberg find significant amounts of C III and O VI. The NEQ ratios have similar distributions at [M/H] $= -1$. Those at solar abundance have significantly more O VI at lower temperatures and similar difficulties matching all of the available ionization states.

O VI-bearing phase for the C III-bearing phase to be at $T \lesssim 10^5$ K. This is very difficult to reconcile with the breadth of the O IV profile, and the limit derived in §3.1.4 for the fraction of that profile that can be associated with hot gas. Of course one may posit a distribution of temperatures, but the models will become increasingly complex and difficult to justify in the face of the relatively simple assumptions that one makes when adopting CIE models. In view of these arguments, pure CIE models are not a good representation of the ionization of this absorber.

Shock-heated WHIM gas may not, however, be in equilibrium. If hot gas cools faster than it can effectively recombine, the gas may be over-ionized for its temperature (e.g., Shapiro & Moore 1976, Edgar & Chevalier 1986, Sutherland & Dopita 1993, Heckman et al. 2002); in addition, if the ion and electron temperatures of shock-heated gas are significantly different, NEQ conditions also hold (see Cen & Fang 2006, Yoshikawa & Sasaki 2006, Bertrone et al. 2008). The comparison of the relative timescales for cooling, ionization, and recombination is a measure of whether such NEQ ionization is important. Tripp et al. (2008) discuss these timescales for the IGM; unfortunately, they could not conclusively argue for or against NEQ effects being important for the WHIM. Recently, Wiersma et al. (2008) have argued that photoionization of metal coolants can suppress cooling in the IGM, increasing the cooling time significantly. If so, this argues NEQ cooling effects are likely not important.

Gnat & Sternberg (2007) have produced NEQ models that follow the ionization fractions of metal ions as gas cools from an initial temperature of $T = 5 \times 10^6$ K. The resulting ionization fractions are metallicity dependent. We have considered models with solar and 10% solar metallicity (see §4.2 and §4.3). For many species, the NEQ models approach the CIE models at low metallicity (Gnat & Sternberg 2007; Tripp et al. 2008), O VI being one of those for which NEQ models at [M/H] $= -1$ are quite similar to CIE models. Given this similarity, it is not surprising that the NEQ models have nearly the same difficulties as the CIE models. The C III/O VI ratio is only matched at $T \approx 1.9 \times 10^5$ K for the Gnat & Sternberg isobaric[6] models at both metallicities, inconsistent with the b-values for C III and with the O III upper limits. Two-temperature NEQ models can be constructed as discussed above for the CIE models, but all require most of the O IV to be associated with gas at temperatures $\sim 2 \times 10^5$ K, which is inconsistent with our component fitting analysis. For solar abundance models, the limit to the O III/C III ratio is requires $T < 2 \times 10^4$ K in the NEQ models, inconsistent with other constraints in this case (e.g., from O II).

Thus, it is unlikely that the gas making up the $z = 0.495$ absorber toward PKS 0405–123 is dominated by collisional ionization. This holds when considering either CIE or NEQ models. If our observations had only measured H I, C III, and O VI, a common situation in IGM observations, these models could possibly be questioned by considering the component structure for this absorber. However, given the low-S/N ratio of these and other STIS observations of the low-z IGM, it would be difficult to strongly rule them out.

4.2 Photoionization Models

The $z = 0.495$ absorber is exposed to the ultraviolet background (UVB) from the integrated light of QSOs and galaxies in the universe. As such, photoionization will play a role in determining the ionization of the gas, which is optically thin to ionizing radiation, even if collisions are the dominant ionization mechanism (Wiersma et al. 2008). Here we consider models in which collisional ionization is unimportant, and the ionization state of the absorber is determined by photoionization alone. In this scenario, the absorber amounts to a metal-enriched Lyα forest cloud.

For optically-thin systems, the ionization state of photoionized gas is primarily determined by the ratio of the ionizing photon to hydrogen volume densities, i.e., the ionization parameter $U \equiv n_\gamma / n_H$, and the spectral shape of the ionizing background. The metallicity can have a minor effect on the ionization through its importance for the thermal balance. We use the Cloudy ionization code (version 07.02; last described by Ferland et al. 1998) to model the photoionization of a plane-parallel slab of gas illuminated by a diffuse UVB. Because this is intrinsically a one dimensional model, it is effectively an infinite thin sheet diffusely illuminated on both sides by the UVB. We stop the calculations when the integrated H I column matches that observed. Our models vary the density for the assumed ionizing spectra (see below), which is akin to varying the ionization parameter. We assume solar relative abundances for the initial models with a base metallicity of [O/H] $= -0.5$ and adjust the metallicity at a later point to best match the total column densities of the ions. The metallicity plays only a small role in the

[6] Gnat & Sternberg 2007 discuss the conditions over which which isobaric or isochoric models are likely to be appropriate. This absorber is near the cross-over point, though more likely to be in the isobaric regime. Isochoric models give very similar results.

relative ratios of the metal ions, although it fixes the ratio of metal ions to H I.

We investigate two possible models for the ionizing background at $z \approx 0.5$ from the Haardt & Madau (2005, in preparation; details given in Haardt & Madau 2001) update to the work by Haardt & Madau (1996). These background spectra, calculated with the CUBA software (Haardt & Madau 2001), assume that: 1) the UVB is dominated by quasars and active galactic nuclei (the QSOs-only spectrum); or 2) the UVB is a combination of light from quasars and integrated light escaping from galaxies (the QSOs+galaxies spectrum).[7] The input QSO spectrum in these models uses a power law index of $\alpha = 1.8$ for wavelengths below 1050 Å (e.g., Zheng et al. 1998, Telfer et al. 2002), while the basic spectral shape for the light leaking from galaxies is based on a spectrum from Bruzual & Charlot (1993, 2003) libraries for a population of stars with 0.2 solar metallicity and 0.5 Gyr age. The ionizing ($h\nu > 1$ Ryd) radiation coming from the galaxies is attenuated by the gas and dust within the galaxies. The escape fraction of ionizing gas from the galaxies is an important quantity for calculating the background, and Haardt & Madau adopt $f_{\rm esc} = 0.1$ in their base model (F. Haardt, 2008, priv. comm.). As noted by Haardt & Madau (2001), the definition of the escape fraction in this model is not the ratio of escaping Lyman continuum photons to those produced by the underlying stellar population. Rather, this value is normalized to the observed (i.e., dust attenuated) 1500 Å flux of galaxies (see Eqn. 1 in Haardt & Madau 2001). In the QSOs+galaxies spectrum, the majority of the hydrogen ionizations are caused by photons that have escaped from galaxies.

Figure 8 shows the results of our photoionization models for the QSOs-only (*left*) and QSOs+galaxies (*right*) spectra. We plot the ratio of column densities of O III, O IV, O V, and O VI to C III from the Cloudy models as a function of the ionization parameter assuming solar relative abundances. The thick solid lines denote regions of the models for which the calculated ratios are consistent with observed column densities. While we have plotted the $N(X)/N(\mathrm{C\ III})$ ratios, the thick lines are for the individual ions are based on all of the available constraints. These plots do not include all of the ions for which we have limits, as many of the model values are well below the upper limits for this absorber. Also, the ions of nitrogen are not used to constrain the ionization. Non-solar N/C or N/O ratios are common at moderately-low metallicities, and we use the N IV column to estimate the N/O ratio in the absorber. When using O IV we have been conservative, since we are concerned that the component fitting results may not fully account for the saturation in the profile; we adopt the lower limit derived from integrating the $N_a(v)$ profile of O IV. The models that fall within 1σ of the component fitting column are also shown with a black line in Figure 8.

The best-fit models for the QSOs-only spectrum has $\log U \approx -1.28 \pm 0.03$, which matches all of the column density constraints from Table 1. The quoted uncertainties in the ionization parameter represent the range over which the models are within 1σ of the observed ratio. The constraints on the models rely on most of the available ions, but the most important are the O VI/C III, O III/O IV, and O IV/O VI ratios. The constraints are significantly less stringent without the inclusion of the O III limits.

The metallicity implied by these models is $[\mathrm{O/H}] = [\mathrm{C/H}] = -0.15 \pm 0.07$, where the uncertainty accounts for the range of ionization parameters and observational uncertainties, but does not attempt to account for any systematic uncertainties associated with the choice of UVB, adopted solar system abundances, missing atomic data, or model assumptions. For our adopted UVB, these models have $n_{\rm H} \approx 5.0 \times 10^{-5}$ cm^{-3} and $\log N(\mathrm{H}) \approx 18.5$, giving a pathlength for the model cloud of $\sim$ 20 kpc. The derived density is similar to the predictions for average Lyα forest cloud of this column density from the models of Schaye (2001) and Davé et al. (1999), both of which predict $n_{\rm H} \approx 10^{-5}$ cm^{-3}. The simulations show a large scatter in the $\rho/N(\mathrm{H\ I})$ relation and have factor of a few type uncertainties. The neutral fraction of hydrogen for this model is $x(\mathrm{H\ I}) \equiv N(\mathrm{H\ I})/N(\mathrm{H}) \approx 6 \times 10^{-5}$. Cloudy predicts equilibrium temperatures $T \approx 28,000$ K for both assumed UVB models.

The best-fit models based on the QSOs+galaxies spectrum match the available constraints for $\log U \approx -0.87 \pm 0.03$, corresponding to $n_{\rm H} \approx 3.5 \times 10^{-5}$ cm^{-3} for this spectrum. The metallicity implied by this model is $[\mathrm{O/H}] = [\mathrm{C/H}] = -0.62 \pm 0.07$, nearly 0.5 dex lower than that derived using the QSOs-only UVB. This model has $\log N(\mathrm{H}) \approx 19.0$, giving a pathlength for the model cloud of $\sim$ 90 kpc. Thus, the fraction of neutral hydrogen is $x(\mathrm{H\ I}) \approx 2 \times 10^{-5}$. The larger ionization fraction of H and ionization parameter in the QSOs+galaxies models comes about because the radiation leaked from galaxies contributes significantly more photons between 1 and 4 Rydbergs. Thus, to produce O IV and O VI columns comparable to those in the QSOs-only models requires more H-ionizing photons (and C III-ionizing photons).

For both choices of UVB, comparing the measured N IV column density with those predicted by the models gives $[\mathrm{N/O}] \approx -0.60^{+0.11}_{-0.16}$. This value of [N/O] is consistent with [N/O] seen in metal-poor galaxies and damped Lyα systems at similar metallicities (see Henry & Prochaska 2007, Pettini et al. 2008). It is difficult to assess the significance of this result given the uncertainties in both the models and the data. Though, given the significant differences in total metallicity between the two UVB models, it is encouraging that both give the same [N/O] results.

We have assumed a solar C/O ratio in the above analysis. Danforth et al. (2006) have made some arguments for $[\mathrm{C/O}] \approx -1$ in low-z O VI+C III systems (their equation 15; see also Danforth & Shull 2008), although they view this result with a great deal of skepticism. We have enough information from the oxygen ions alone to test whether the present absorber has such a low value. Using only the oxygen ions to constrain models using the QSOs-only UVB, the ionization parameter is constrained to be $\log U = -1.36 \pm 0.10$. This model gives $[\mathrm{O/H}] = 0.0 \pm 0.2$, i.e., solar abundance, with $[\mathrm{C/O}] = -0.2 \pm 0.1$ and $[\mathrm{N/O}] = -0.7 \pm 0.2$. Adopting the QSOs+galaxies model leads to $\log U = -0.92 \pm 0.10$. This model gives $[\mathrm{O/H}] = -0.5 \pm 0.2$, $[\mathrm{C/O}] = -0.1 \pm 0.1$ and $[\mathrm{N/O}] = -0.7 \pm 0.2$. Thus, for these assumed UVB, the data do not support a C/O ratio as low as 0.1 times solar.

A slightly sub-solar C/O abundance is consistent with our models, although solar C/O is not ruled out. Allowing the C/O to be subsolar affects the derived [O/H] abundances moderately. Notably, the QSOs-only model produces a solar oxygen abundance, which seems unlikely for an absorber arising in the diffuse IGM; however this absorber, given its large O VI column, may arise near to a galaxy. We will discuss the implied abundances further in §5.

[7] One could imagine that the absorber were near to an individual galaxy and estimate the ionizing spectrum seen from that galaxy as a function of distance as, for example, Fox et al. (2005) have done for studying high velocity clouds about the Milky Way. The present models attempt to study the effects of the integrated light escaping from the overall population of galaxies.

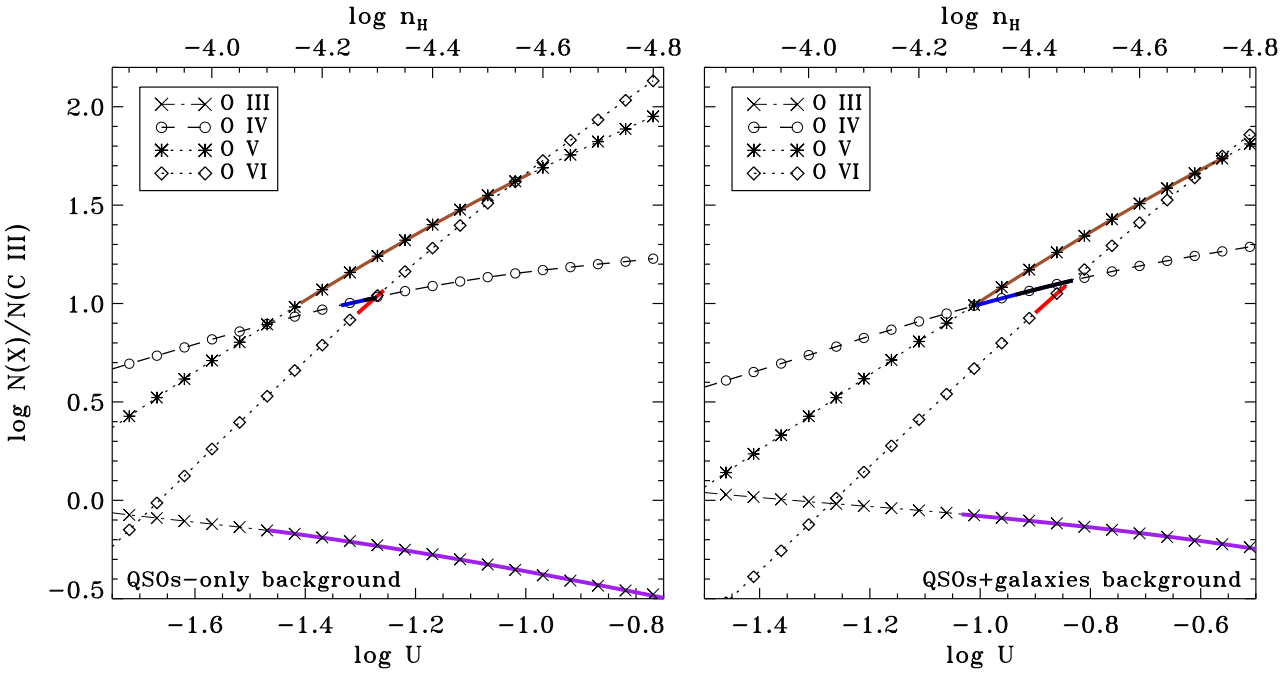

Figure 8. Photoionization models for the $z = 0.495$ absorber toward PKS 0405–123 assuming an ionizing background dominated by QSO radiation (*left*) or a background that also contains a contribution from galaxies (*right*). The column density ratios of several ions relative to C III are plotted, with the solid lines representing regions over which the models are consistent with all of the observed column density ratios and limits (i.e., not just with C III as plotted here). For O IV, we show the region allowed if one adopts the component fitting results as the thick grey line. For our assumed UVB intensities, the densities implied by the ionization parameters are given across the top of each plot. The models shown assume a metallicity of [M/H]$= -0.15$ and -0.62 for the QSOs-only and QSOs+galaxies backgrounds, respectively. The metallicity has a small effect on the ionization balance and, hence, only a small impact on these plots which show relative metal ion column densities. We assume solar relative abundances for C/O. The best-fit models assuming a QSOs-only background give $\log U \approx -1.28$ while the models with a QSOs+galaxies background give $\log U \approx -0.87$.

4.3 Multiphase Models

We have shown above that a pure photoionization model can match the constraints provided by the ionic column densities in this absorber. Even the O VI can be adequately explained by photoionization by the diffuse UVB. The C III and O IV profiles are well fit with relatively narrow components (see Table 2) implying low temperature gas consistent with photoionization, although we have some concern about the limits from the O IV fits as discussed above. The component structure of O VI is not as clearly delineated. This may simply be due to the low signal-to-noise of the observations, but could also imply broader components in O VI than the lower ions. The O VI/C III ratio varies somewhat with velocity in the profile, albeit at moderate significance. Furthermore, there is room within the O IV profile for a broad component tracing warm-hot gas ($T \gtrsim 10^5$ K) that contributes as much as $\sim 30\%$ of the O IV column. The breadth of the C III profile suggests high-temperature collisionally-ionized gas cannot be important for that ion (and, indeed, this is not expected; see Prochaska et al. 2004). While the evidence is not firm, this absorber could plausibly contain regions of differing metal ion ratios and perhaps different ionization mechanisms and temperatures (§3.1.4). The evidence for multiphase absorption is certainly not as clear-cut as some cases, for example, emphasized in the Tripp et al. (2008) survey of low-z systems.

Here we consider a multiphase model for the ionization of the $z \approx 0.495$ absorber. In our model, the column densities are predicted using a linear combination of the pure collisional ionization and photoionization models considered above (see, e.g., Prochaska et al. 2004). The free parameters are the ionization parameter of the photoionized component, the temperature of the collisionally ionized component, the fraction of the total hydrogen column associated with the collisionally ionized medium, $\phi_{\rm coll}(\rm H)$, and the metallicity of the gas, assumed to be the same between phases. This is meant as a crude model of a cool, photoionized cloud surrounded by shock-heated hot gas. We note that this model is not self-consistent in that neither is the collisionally-ionized phase is itself not subjected to an ionizing radiation field nor is the photoionized phase subject to radiation from the hot, collisionally-ionized phase. We are thus assuming that collisional processes so dominate the ionization of the hot phase that the UVB does not have a significant impact on this phase while the radiation from that hot phase is not intense enough to rival the UVB in importance for the photoionized phase.

The results of these models are shown in Figure 9, which shows the range of allowed values for $\phi_{\rm coll}(\rm H)$, $\phi_{\rm coll}(\rm O\ VI)$, and $\log N(\rm H)$ as a function of temperature for models adopting the QSOs-only or QSOs+galaxies spectra of Haardt & Madau (2005, in preparation) and Gnat & Sternberg (2007) CIE models. Here $\phi_{\rm coll}(\rm H)$ and $\phi_{\rm coll}(\rm O\ VI)$ are the fractions of the total H and O VI columns that arise in the hot, collisionally-ionized gas. These models assume that $\lesssim 30\%$ of the O IVarises in the collisionally-ionized phase (i.e., $\phi_{\rm coll}(\rm O\ IV) \leqslant 0.3$). If this limit is relaxed, a broader range of contributions from the hot, collisionally-ionized phase is allowed for temperatures $\log T \lesssim 5.6$, although the higher temperature results are not much affected. These models assume CIE, but the NEQ models give results that are not significantly different. Our calculations extend over the temperature range $4.5 \leqslant \log T \leqslant 6.5$, although models for $\log T \lesssim 5.30$ ($T \lesssim 2 \times 10^5$ K)

did not produce models in agreement with the observations. The ionization parameters are not shown because they differ little from the values derived in the pure photoionization models discussed above (§4.2). Because we are interested in the origins of the O VI, these plots only show models for which $\phi_{\rm coll}({\rm O\ VI}) \geqslant 0.05$. This is the cause of the apparent lower limit to the total H column densities. If we do not require that the collisionally-ionized phase contribute to the O VI column densities, the lower right of the top and bottom panels in these figures would both be allowed (see §5).

We find multiphase models that are consistent with our observational constraints for $T \gtrsim 2.2 \times 10^5$ K ($\log T \gtrsim 5.35$) for both adopted UVB spectra. The ionization parameters appropriate for the photoionized phase are similar to those reported in §4.2. They differ from the pure photoionized models by up to -0.2 dex and $+0.05$ dex, i.e., the maximum excursions are to lower ionization parameter. For temperatures $T \sim 2.8 \times 10^5$ K to 5×10^5 K ($\log T \approx 5.45$ to 5.70) we have very little constraint on the fractions of H or O VI arising in the collisionally-ionized gas, largely because we only have limits to the O IV/O VI ratio. Thus, there is a degeneracy between the collisionally-ionized phase and the photoionized phase for the oxygen ions where one phase may compensate for the other. The C III still arises almost exclusively in the photoionized phase.

The metallicities in these mixed-phase models are very similar to those derived from pure photoionization models. The range of allowed metallicities for the QSOs-only UVB models is [O/H] ~ -0.33 to -0.05; for the QSOs+galaxies UVB we find [O/H] ~ -0.76 to -0.52. This is quite insensitive to the assumptions for $T \gtrsim 5 \times 10^5$ K ($\log T \gtrsim 5.7$) since the collisionally-ionized phase contributes little to the detected ions, which are all associated with the photoionized phase save for a small fraction of O VI.

Thus, a simple multiphase model with distinct collisionally-ionized and photoionized regions allows for significant amounts of hot gas. For temperatures $T \gtrsim 5 \times 10^5$ K this is due to the nature of the observational constraints. We do not detect Ne VIII or Mg X, and these are the only ions covered by our observations with significant ionization fractions at these temperatures. At temperatures $T \sim 2.8 \times 10^5$ K to 5×10^5 K ($5.45 \lesssim \log T \lesssim 5.70$), the fraction of the total column of hydrogen allowed to be associated with the collisionally ionized phase may be significant and is poorly constrained. We find none of these models match all of the available constraints for a collisionally-ionized phase at temperatures $T \lesssim 2 \times 10^5$ K.

Another type of multi-process model is one in which gas at a fixed temperature is irradiated by the UVB (e.g., Tripp et al. 2008, Danforth et al. 2006). In this approach, we fix the gas temperature within our Cloudy models, which provides for collisional ionization, and calculate the ionization balance for a range of ionization parameters at each temperature. This is effectively a collisionally-ionized gas that is modified by the UVB ionization. For both UVB models investigated here the models are only able to match the available constraints for $T \lesssim 40,000$ K, consistent with the b-values of components seen in C III. The main difficulty is in avoiding overproduction of O III at high temperatures. The allowable ionization parameters, set by the O VI/C III ratio, are similar to those discussed above, with $\log U \approx -0.85 \pm 0.05$. This model also gives a similar abundance with [O/H] $\approx -0.70 \pm 0.05$. Similarly, the models assuming a QSOs-only UVB spectrum give [O/H] $\approx -0.27 \pm 0.05$ at $\log U \approx -1.23 \pm 0.05$. A single temperature collisionally-ionized gas exposed to the UVB, then, is inconsistent with our observations for the large temperatures consistent with the WHIM, $T \sim 10^5$ to 10^7 K. Indeed, the temperatures allowed by this approach are generally so low that they approach those produced by a pure photoionization model (which gives $T \sim 28,000$ K).

5 DISCUSSION

We have presented measurements of five metal ions and limits on another eight in the $z \approx 0.495$ absorber toward PKS 0405–123. We have discussed a range of possible ionization mechanisms, determining that this absorber may be described by a pure photoionization model, but may also harbor some collisionally ionized material at $T \gtrsim 10^5$ K if it is mixed with a cool photoionized component.

5.1 The WHIM and Low-z O VI Systems

Intervening O VI absorption line systems are quite common at low redshifts, with $dN/dz \approx 10 - 20$ for $W_r \gtrsim 30$ mÅ (Danforth & Shull 2008; Tripp et al. 2008; Thom & Chen 2008) depending on the criteria used to select the O VI systems. Thus, they probe a significant baryon reservoir no matter their origin. However, they have elicited the most interest due to the possibility that they trace the "missing baryons" associated with a WHIM. For systems with $W_r \gtrsim 200$ mÅ like the one studied here, the absorber density is significantly lower, of course, with $dN/dz \approx 2$ (Tripp et al. 2008).

Some intervening absorbers with significant O VI absorption likely do trace the WHIM. These may be absorbers with signatures of pure collisionally ionized gas at high temperatures, such as the systems at $z \approx 0.31978$ toward PG 1259+593 from Richter et al. (2004) or at $z \approx 0.1212$ toward H1821+643 discussed by Tripp et al. (2001), in which O VI and H I have breadths consistent with $T \approx (2-3) \times 10^5$ K. These may also be found in absorbers that are part of a multiphase structure including a very hot component ($T \gtrsim 5 \times 10^5$ K) such as the Ne VIII-bearing system at $z \approx 0.207$ toward HE 0226-4110 (Savage et al. 2005). There are reasonable arguments for the origins of other absorbers in hot shock-heated gas, such as the $z \approx 0.056$ systems toward PKS 2155–304 that Shull et al. (2003) have argued trace material infalling onto a group of galaxies (which may exhibit X-ray absorption; Fang et al. 2002). However, for most O VI absorbers, the connection to the WHIM is less evident or non-existent (Prochaska et al. 2004, Lehner et al. 2006). In their survey of $z \lesssim 0.4$ O VI systems, Tripp et al. (2008) find $\gtrsim 34\%$ of their intervening absorbing components are associated with cool gas at $T < 10^5$ K based on an analysis of b-values. Thus, a significant fraction are obviously too cool to be associated with the $T > 10^5$ K WHIM, although they may represent cooled WHIM material (e.g., Kang et al. 2005). However, $\sim 50\%$ of that sample shows significant differences between the H I and O VI profiles, suggesting a multiphase structure. Such absorbers could include gas at $T \gtrsim 10^5$ K.

While the origins of O VI in the IGM may be ambiguous, with photoionization being a significant contributor to the O VI in a significant number number absorbers (e.g., Tripp et al. 2008, Thom & Chen 2008b, Oppenheimer & Davé 2009, Kang et al. 2005), the Li-like ions Ne VIII and Mg X, which peak in abundance in CIE models at $T \sim 6.4 \times 10^5$ K and 1.1×10^6 K, respectively (Gnat & Sternberg 2007), are much more secure probes of shock-heated hot gas. These ions are probes of WHIM material at temperatures where a significant fraction of the low-z baryons are expected to reside (Davé et al. 2001) and probe gas in the temperature regime accessible via X-ray absorption studies ($5 \times 10^5 < T < 3 \times 10^6$

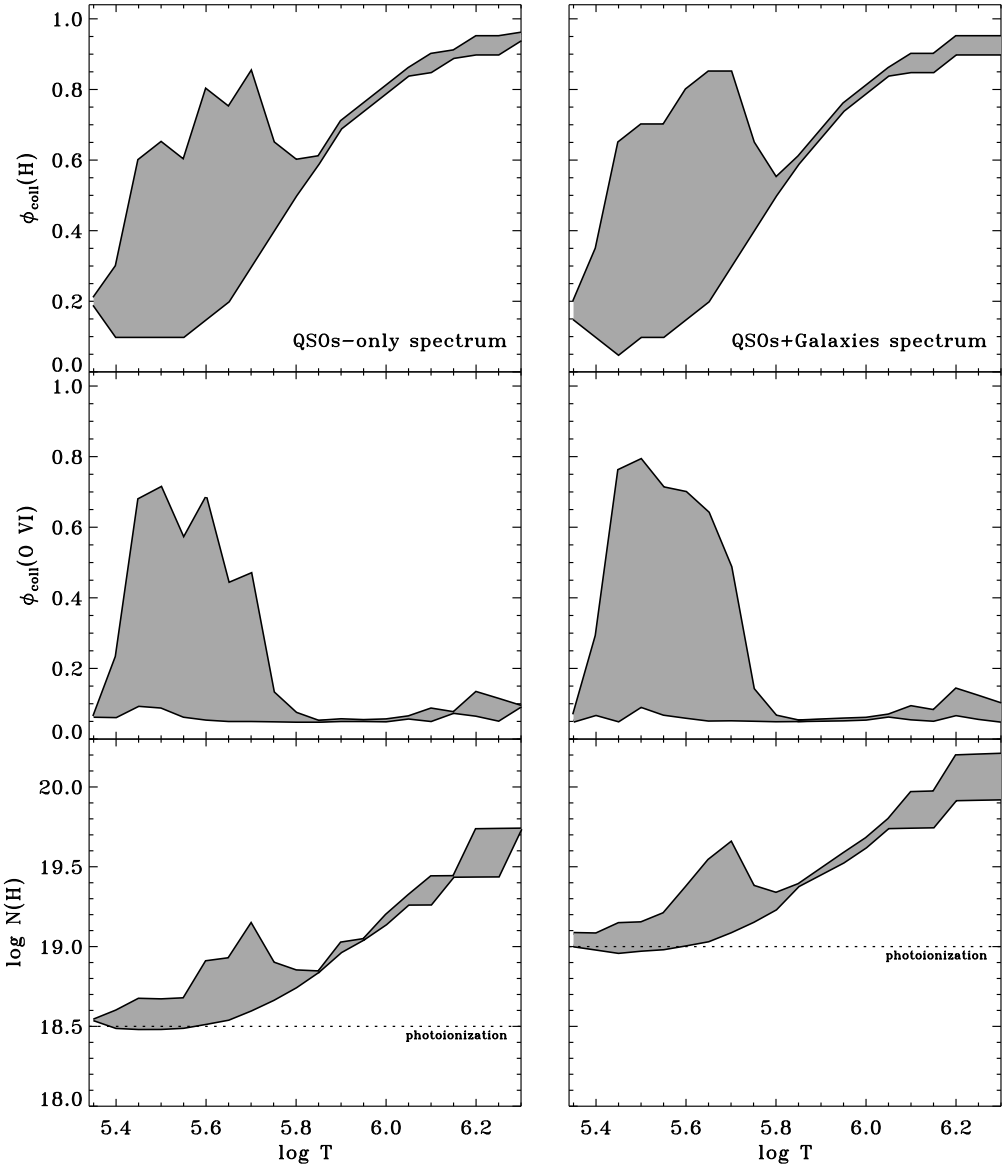

Figure 9. Allowed regions of parameter space for multiphase models assuming $\phi_{\rm coll}(\text{O IV}) \leqslant 0.3$. For both the QSOs-only UVB (*left*) and QSOs+galaxies UVB (*right*) we show the range of allowed values for $\phi_{\rm coll}(\text{H})$, $\phi_{\rm coll}(\text{O VI})$, and the total $\log N(\text{H})$. The values of $\log N(\text{H})$ at $\log T \gtrsim 5.7$ are largely set by the limits on Ne VIII and Mg X under the assumption of collisional ionization. At these temperatures, these are the only ions that provide constraints on the collisionally ionized phase, although we have required $\phi_{\rm coll}(\text{O VI}) \geqslant 0.05$. The $\phi_{\rm coll}(\text{H})$ and $N(\text{H})$ curves are upper limits for temperatures $\log T \gtrsim 5.7$ if one does not require the gas to contribute significantly to the O VI profiles. These figures include H columns from both the photoionized and collisionally-ionized phases. The columns predicted by a pure photoionization model are shown as the dotted lines. The total column density limits for the WHIM are summarized below.

K). The absorber considered here is one of the few O VI absorbers for which Ne VIII could be searched (Prochaska et al. 2004, Richter et al. 2004, Savage et al. 2005, Lehner et al. 2006), and the only one for which a limit on Mg X is currently available. A summary of previous observations of Ne VIII in the low-z IGM is given in Table 7 of Lehner et al. (2006). Ne VIII has only been detected in the multiphase absorber at $z \approx 0.207$ toward HE 0226−4110 (Savage et al. 2005), the system with the second highest $W_r(\text{O VI}\,1031) = 169 \pm 15$ mÅ among those yet searched for Ne VIII (the highest being the current absorber). Savage et al. derive $N(\text{Ne VIII})/N(\text{O VI}) = 0.33 \pm 0.10$ for this absorber with $\log N(\text{O VI}) = 14.37 \pm 0.03$.

Our 3σ limit to the Ne VIII column density gives the lowest limit on this ratio yet observed, $N(\text{Ne VIII})/N(\text{O VI}) < 0.18\,(3\sigma)$ assuming the O VI derived from integrating the full profiles (see §3.1.3); a slightly higher value of < 0.21 is derived if using the O VI in the velocity ranges of components 1, 2, and 3. The O VI

equivalent width of this system is 25% larger than that for the $z \approx 0.207$ absorber toward HE 0226−4101.

The lack of Ne VIII and Mg X absorption in the $z \approx 0.495$ absorber toward PKS 0405–123 implies that there is not a very large reservoir of hot [$\sim (0.5-3) \times 10^6$ K], collisionally ionized gas associated with this absorber, although the precise limits depend on the temperature of the gas. Such hot gas would not be detectable in the other ions probed by our observations due to its high temperature (and hence ionization state). Figure 10 shows limits to the total H column density as a function of temperature for gas associated with the WHIM in this absorber assuming [M/H]≈ -0.62 (from the models adopting a QSOs+galaxies UVB). The distribution of these limits with temperature arises from jointly considering the O VI, Ne VIII, and Mg X ionization fractions and observational limits on their columns. The limits from the individual ions assuming CIE are shown by the gray lines. At $\log T < 5.7$, we assume the results from Figure 9 for a multiphase absorber. The H column density limits displayed in Figure 10 are lower if one assumes a higher metallicity (e.g., from models with the QSOs-only UVB).

Two things are important from this figure. First, if additional hot gas is present with temperatures $\log T \lesssim 6.5$, it would not provide sufficient column to lead to detectable X-ray absorption except perhaps along the sight lines to the very brightest sources. Over the range $6.0 \leqslant \log T \leqslant 6.5$, we infer the O VII K$\alpha$ line should have an equivalent width $W_r < 6$ mÅ to $W_r < 15$ mÅ with a column $\log N(\mathrm{O\ VII}) \lesssim 16.7$ (all 3σ limits). These are derived from the limits on Ne VIII and Mg X, assuming assuming CIE ionization fractions and solar relative abundances (the absolute abundance is not important since the O VII column is predicted from other metal species). We also assume pure thermal broadening of the lines. O VIII Kα would be even weaker, with a maximum of $W_r < 5$ mÅ and $\log N(\mathrm{O\ VII}) \lesssim 15.75$ for $\log T \sim 6.5$. The presence of O VII at the equivalent width limit for the highest temperatures might be marginally detectable toward bright objects (e.g., Williams, Mathur, & Nicastro 2006, Fang et al. 2007), although this is a 3σ limit and absorption is very unlikely to be present at that level. Furthermore, the discrepancies discovered between various instruments and groups for X-ray absorption lines reported at good significance toward extremely bright objects makes it difficult to imagine the current absorber could be reliably detected if at $\log T \lesssim 6.5$ (e.g., see discussion in Bregman 2007). Second, the limits for WHIM material at $\log T \gtrsim 6.5$ are quite limited due to low ionization fractions of even these highly-ionized species at such temperatures. The majority of the metal-bearing WHIM is thought to be at temperatures below this (e.g., Davé & Oppenheimer 2007), with higher temperature IGM gas tracing large overdensities associated with clusters. At $\log T \sim 7$, both the O VII and O VIII transitions are limited to $W_r \lesssim 20$ to 25 mÅ (3σ). We note that photoionization models for this absorber, which can match the available constraints quite well, predict $\log N(H) \sim 18.5$ to 19.0.

The Li-like ions limit the column of very hot gas in this absorber over a temperature range at which the majority of the WHIM baryons are expected to reside to be relatively low. And while some of the gas in this absorber could be associated with a few$\times 10^5$ K gas, a significant cool photoionized component is needed to explain the lower ionization species such as C III. The O VI in this system may be described fully by a photoionized gas. However, even if some of the O VI is produced via collisional ionization, the absorber must include some photoionized material (with $\sim 50\%$ or more of the O VI coming from a cool photoionized phase). Because of the uncertainties in its origins, O VI is not a robust, pure tracer of the WHIM in this absorber. There is no direct evidence for hot gas with $T \gtrsim 10^5$ K material in this absorber, even though it has very strong O VI. For temperatures $T \gtrsim 5 \times 10^5$ K, however, the gas would only be seen in Ne VIII or Mg X absorption.

The absorber studied here may have a multiphase structure, where the high-temperature shock-heated gas contributes somewhat more than half of the total H column density (unless at $T \gtrsim 5 \times 10^5$ K, in which case we have few constraints on the gas). Tripp et al. (2008) note that $\approx 50\%$ of their intervening absorbers show strong differences between the H I and O VI profiles, evidence for a possible multiphase structure. The evidence from the velocity profiles of the absorption for a multiphase structure to this system is slight at best. While the O VI/C III seems to vary somewhat between components 1 and 2, this does not necessarily imply these components have significantly different ionization mechanisms and temperatures.

The multiphase absorbers noted by Tripp et al. typically show large discrepancies in the velocity distribution of H I and O VI absorption and/or differences in the characteristics of the detected low-ionization metals compared with O VI. If the present absorber does have a mixture of phases, it may indicate that the fraction of the low-z O VI systems with multiphase structure is larger than Tripp et al. estimate. The presently available observations from STIS and *FUSE* do not probe a broad enough range of ions or measure the velocity-resolved profiles with enough signal-to-noise to constrain the structure of many systems. Future observations with the Cosmic Origins Spectrograph will provide much higher quality spectra, allowing us to detect weaker lines and study the velocity profiles at higher signal-to-noise (albeit at lower resolution than STIS). In particular, observations of C IV would provide significant diagnostic power (see below); better quality observations of the H I transitions could allow a search for broad components therein.

Simulations generally predict that the high O VI equivalent width systems like the present absorber are the most likely to arise in the hotter gas, either the diffuse WHIM or gas in higher overdensity regions including galaxy halos (Oppenheimer & Davé 2009, Ganguly et al. 2008, Kang et al. 2005, Davé et al. 2001). The environment of the absorber is pertinent to its origins, and a number of works have explored the connection between O VI absorbers and galaxies (e.g., Wakker & Savage 2009, Cooksey et al. 2008, Lehner et al. 2008, Stocke et al. 2006, Tripp et al. 2006, Tumlinson et al. 2005, Sembach et al. 2004). Prochaska et al. (2006) have presented a galaxy redshift survey for the sight line to PKS 0405–123 (see also Williger et al. 2006). The surveys of this sight line are so far inadequate to bear on the relationship of this absorber to galaxies. Prochaska et al. find only three $L \sim 6L_*$ galaxies within 1000 km s^{-1} of the absorbers. Two of these galaxies are found within $\sim$ 200 km s^{-1} of the absorber, but at impact parameters $\rho \gtrsim 10$ Mpc. This survey is $> 80\%$ complete to $R = 21$ (or roughly $L \sim 0.8L_*$) and 70% complete to $R = 22$ ($\sim 0.3L_*$). No galaxies aside from the three high luminosity systems are found at this redshift. So, if this system is associated directly with a galaxy, the galaxy is likely to be of order $L \sim 0.1L_*$ or less. This absorber is not at so high a redshift that it is impractical to eventually study the fainter galaxies near this absorber with 8-m to 10-m class telescopes.

5.2 Abundances and Ionization Mechanisms in the Low-z IGM

The metallicity of low-z IGM absorbers has been the subject of much work over the last decade. The abundance distribution of the IGM can be used to probe the extents over which galaxies expel

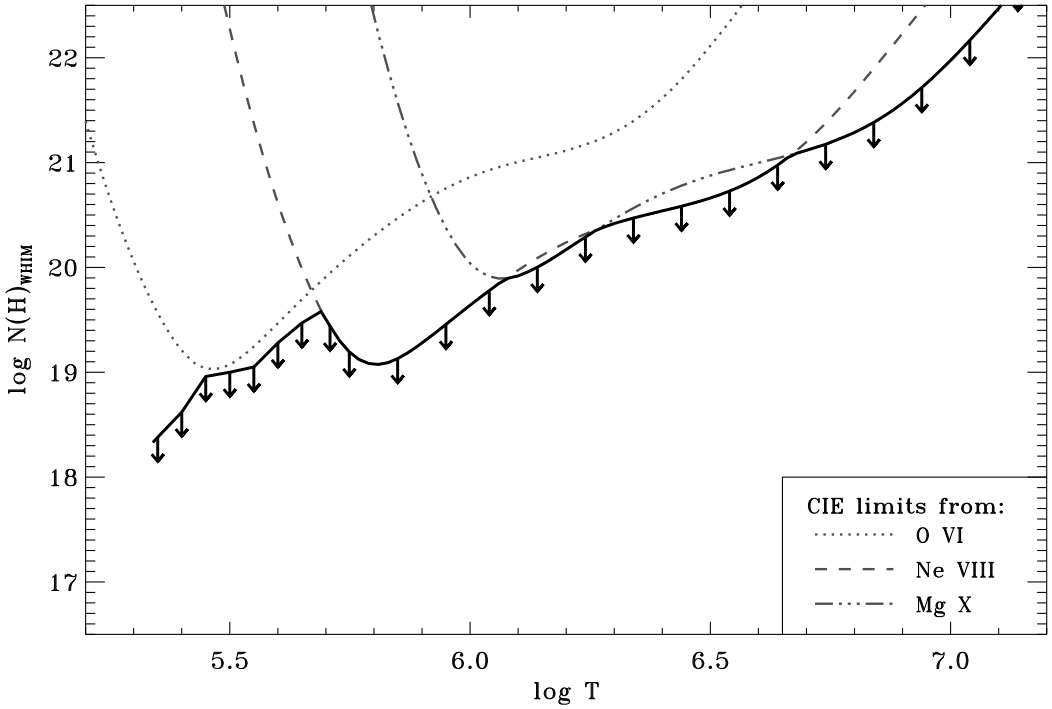

Figure 10. Limits on the collisionally-ionized WHIM column density of this absorber as a function of temperature based on limits on the column densities of O VI, Ne VIII, and Mg X assuming CIE ionization fractions with an abundance of [M/H] $= -0.62$ (see §4.2 and §4.3). The species-dependent limits for CIE are shown with the dashed curves. At temperatures $\log T < 5.7$, the limits are from the multiphase analysis discussed in §4.3 (see also Figure 9). These limits are dependent on the assumptions of those models. We note that for $6.4 \lesssim \log T \lesssim 7.0$, O VII has an ionization fraction of nearly unity in the models considered. Over that range the column of this ion is simply 4.4 dex below the column of hydrogen plotted here for our assumed abundances. Higher assumed abundances will lower the H column density limits.

metals, whether the metals escape the galaxies or fall back onto them, and the impact of such metal expulsion on galaxy evolution (e.g., Davé & Oppenheimer 2007, Calura & Matteucci 2006, Tumlinson & Fang 2005). The level of metal enrichment then suggests the sphere of influence over which galaxies affect the IGM, and it is an important consideration when using metal lines to calculate the baryon density of low-z IGM absorbers since in this case $\Omega_b \propto Z^{-1}$ (e.g., Tripp et al. 2008, Thom & Chen 2008a, Danforth & Shull 2008).

Many low-redshift metal line absorbers tend to show metallicites between [M/H] ≈ -1 and 0 (Cooksey et al. 2008, Tripp et al. 2006, Aracil et al. 2006, Lehner et al. 2006, Prochaska et al. 2004), although lower metallicities are found as well (e.g., Stocke et al. 2007 and previous references). The median metallicity in the higher redshift $z \approx 2-3$ LAF is [M/H] $\lesssim -2$ (e.g., Aguirre et al. 2008; Simcoe, Sargent, & Rauch 2004; Schaye et al. 2003), although Simcoe et al. (2006) find that the small fraction of the IGM nearest to galaxies is at metallicities close to those found at low-z. Generally it is thought that significant pollution of the average diffuse IGM has to have occurred since $z \sim 3$ (Stocke et al. 2007, Davé & Oppenheimer 2007, Tumlinson & Fang 2005).

Generally speaking there are three uncertainties associated with the ionization of the $z \approx 0.495$ system toward PKS 0405–123 (and others): 1) Is the source of the ionization collisional ionization, photoionization, or a mixture of both? 2) If photoionization is important, what is the nature of the ionizing UVB spectrum? and 3) If collisions are important, what assumptions are appropriate (e.g., CIE versus various NEQ scenarios) and are the models sufficiently sophisticated? Of course, the latter concern of the level of sophistication in the models is appropriate for all processes. The $z \approx 0.495$ absorber toward PKS 0405–123 has characteristics consistent with pure photoionization by the UVB, perhaps including contributions radiation that has leaked from galaxies (Haardt & Madau 2001). Models of pure collisional ionization do not reproduce the observed ionic ratios in this absorber. Multiphase models that include the effects of ionization via both photons and electron collisions are also broadly consistent with the observed ionic ratios in this absorber. Even in these models, however, the majority of the gas is likely warm photoionized material.

The choice of one or the other of the ionizing backgrounds considered here is an important one, as they give significantly different metallicities for the absorber, ranging from [O/H] ≈ -0.62 for the QSOs+galaxies UVB to ≈ -0.15 for the QSOs only spectrum. Thus, the choice of one of two reasonable UVB spectra (and other UVB prescriptions exist) gives metallicities discrepant by ~ 0.5 dex, or a factor of three. The difference comes about because the QSOs+galaxies model requires more H-ionizing photons to match the O VI column. Thus, for the same O IV/O VI or O VI/C III ratio, the neutral fraction, x(H I), is lower in the QSOs+galaxies model, implying a larger total H column density for the same metal ion columns. This difference can have significant consequences for understanding the enrichment of the low-z IGM and the low-z baryon budget.

Thus there is a large systematic uncertainty associated with the choice of ionizing background model (e.g., see discussions in Tripp et al. 2008, Schaye et al. 2003, Giroux & Shull 1997), one

that is not always explicitly considered in the study of the low-z IGM. There are several plausible UVB models available, such as those dominated by AGN or QSOs with varying spectral slopes (e.g., Telfer et al. 2002, Mathews & Ferland 1987) or those containing contributions from ionizing radiation that has escaped galaxies (e.g., the Haardt & Madau spectrum adopted here).

Determining the spectral shape of the UVB is an on-going challenge. We have shown that the $z \approx 0.495$ absorber toward PKS 0405–123 can plausibly be ionized via photoionization by a UVB including a contribution from galaxies with $f_{\rm esc} \sim 0.1$. There is some evidence for a significant contribution to the UVB from galaxies. Faucher-Giguère et al. (2008) have recently presented evidence based on the ionization rate of the $z \sim 2-4$ LAF that galaxies may dominate the ionizing UVB over much of that range, although the extent to which they contribute at low redshift is less well constrained.

The UVB may also be spatially variable, depending on the proximity of the absorber to galaxies or AGN; thus, the specific shape adopted may depend on unknown properties of the absorber. Reimers et al. (2006) have argued such variation is likely for $z \approx 2$ O VI absorbers, and there is strong evidence for a varying UVB spectral shape from the He II forest at $z \approx 2.5$ (e.g., Shull et al. 2004, Kriss et al. 2001). Oppenheimer & Davé (2009) have also argued for a spatially-variable ionizing background in order to explain the broad range of observed O VI/ H I ratios (Tripp et al. 2008, Thom & Chen 2008b) compared with their simulations. If the UVB can have significant contributions from relatively local sources, leaky low luminosity galaxies ($L \lesssim 0.1L_*$) are mostly likely to influence the ionization of the present absorber given the lack of high luminosity galaxies with low impact parameter to the QSO sight line (Prochaska et al. 2006; see §5.1).

Our data do not provide sufficient diagnostics to distinguish between the two UVB models investigated here. One would ideally like to use a large number of ionic measurements to constrain the contribution of galaxies to the UVB and the spectral slope of the higher energy component dominated by QSOs. A larger sample of low-z absorbers for which several ionization stages of oxygen can be measured will be collected with the upcoming Cosmic Origins Spectrograph; these may be useful in discriminating UVB spectral shapes. The transitions from O II, O III, O IV, and O V are shifted into the COS bandpass for redshifts $z \approx 0.38$, 0.38, 0.46, and 0.83, respectively. Thus, one will have access to O II – O IV+O VI for $z \sim 0.5$ absorbers with COS. As discussed below, the addition of C IV observations so that multiple ionization stages of both C (C II, C III, and C IV) and O are measured may also help distinguish various models for the UVB. Unfortunately, C IV will reside in the NUV channel of COS for absorbers $z \gtrsim 0.12$; the NUV channel is significantly less efficient than the FUV channel (both in throughput and spectral coverage per exposure). Until better constraints on the UVB are available, it seems important that elemental abundance studies of low-z IGM absorbers consider variations in the assumed energy distribution of their adopted UVB when deriving metallicities.

Based on their measurements of H I, C III, and O VI, Danforth et al. (2006) argued that no single phase model can appropriately match their observations. Danforth et al. considered only an AGN-dominated spectrum (though not the one adopted here). We have shown that a single phase photoionization model can match a broad suite of ionic column densities in the present absorber. Other studies have shown that pure photoionization can be made consistent with the ionization characteristics of a significant fraction of the low-z O VI absorbers. For example, Tripp et al. (2008) showed that the O VI/H I and O VI/C III column density ratio in a large sample of absorbers could be explained by simple photoionization models. In their simplest models, they assumed the absorbers have densities consistent with hydrostatic equilibrium in the low-z IGM (following Schaye 2001) and could match the full range of O VI/H I ratios if admitting a significant dispersion of densities about the mean, a range of metallicities, and/or spatially varying UVB intensity and shape, none of which is ruled out at this point. Matching the C III/O VI ratio in the few absorbers for which Tripp et al. had measurements of that ratio required a departure from the hydrostatic assumption, but their assumptions were still reasonable in the context of the IGM.

Thus, Danforth et al. (2006) conclude photoionization is unlikely on the basis of a photoionization model matching an ensemble of absorbers with a small number of ionic measurements to ionization models that use only one UVB that photoionization. Meanwhile, Tripp et al. (2008) come to opposing conclusions, finding that photoionization may explain the conditions in an ensemble of aborbers by comparing a wide range of models using different UVB and density assumptions to an ensemble of O VI and C III measurements. It seems very difficult, given the work on the present absorber, to rule out either photoionization or collisional ionization in such a broad range of absorbers, especially given the small number of ions typically measured and the large number of potential model assumptions.

Danforth & Shull (2008) have presented measurements for a broader range of ions, including C III, C IV, N V, O VI, Si III, and Si IV, in a survey of low-z absorbers. On the basis of an intercomparison of the various ionic ratios, these authors argue that O VI and N V are reliable tracers of the WHIM, while C IV may arise from either collisionally-ionized or photoionized material. The rest of the ions they argue are relatively good tracers of photoionized matter. We feel that detailed models of the individual absorbers are likely required to determine whether this is truly the case (e.g., Cooksey et al. 2008; Prochaska et al. 2004), especially given the range of potential ionizing backgrounds and the potential for mixed ionization processes (photoionization and collisional ionization). In particular, we do not find the argument that the slopes of the frequency distributions in O VI and C III differ a strong argument for the dominance of collisionally-ionized O VI, since a distribution of densities, ionization parameters, and local shape of the UVB may provide for much of the difference. We are not arguing that all of the O VI is photoionized, but rather that it may be difficult to tell even in absorbers with observations of a wide range of ions.

Thus, while there is strong evidence that some of the O VI absorbers are associated with hot, collisionally ionized gas (e.g., Richter et al. 2004, Savage et al. 2005, Tripp et al. 2001), a significant fraction of these systems may be strongly influenced by photoionization, like the present system, which requires $\sim 25\%$–100% of the O VIto be photoionized. These populations are not exclusive given the multiphase nature of some absorbers and the possibility that some trace moderate temperature ($T < 10^5$ K) photoionized gas that is mildly shock heated or that has cooled from higher temperatures (e.g., models discussed by Oppenheimer & Davé 2009, Kang et al. 2005, Furlanetto et al. 2004 and others). Tripp et al. (2008) present temperature estimates for a number of the well-aligned systems in their sample. For those abosrbers with $T < 10^5$ K, a fair number seem to have temperatures somewhat higher than one would expect from pure photoionization, suggesting an extra source of heating that would likely impact the ionization as well. These measurements suggest a mixture of processes could be at work in some absorbers, although photoionization is likely a strong

component for a large fraction of the aligned systems. It is not yet clear what the mixture is like in the multiphase absorbers so categorized due to differences in the H I and O VI profiles.

Prochaska et al. (2004) have noted an apparent anticorrelation between the ionization parameter for the Cloudy photoionization model best fitting the metal column densities and the H I column of an absorber, a result also seen by Lehner et al. (2006) in a larger number of absorbers along several sight lines. This can be understood in part if the H I column is a rough measure of physical density of the absorber (e.g., Schaye 2001; see discussion in Prochaska et al. 2004). The relationship seen in these earlier works will certainly depend on the adopted ionizing spectrum, since the two UVB spectra investigated here give significantly different ionization parameters. However, while those studies adopt a Haardt & Madau QSOs-only spectrum, if this result is directly tied to the physical density of the absorption, the relationship should still hold if galaxies contribute to the ionization. While it has been suggested this correlation implies the absorbers in those studies are likely to be photoionized, our multiphase models show that a mixture of ionization mechanisms can not only give similar ionization parameters for the photoionized component, but in some cases a photoionization only and multiphase ionization model cannot be distinguished. Thus, the correlation likely does not rule out a contribution to those absorbers from collisional ionization, although it may suggest photoionization dominates the ionization, as in the absorber studied in this work.

An important remaining question is how one might distinguish multiphase models such as those with results summarized in §4.3 from the pure photoionization models of §4.2. While the aforementioned ionization parameter-H I column relationship may not discriminate between these models, there are several promising options. For the current absorber, C IV has significant power to discriminate between these classes of models. The ratios C IV/C III and C IV/O VI are significantly different for photoionization models compared with the multiphase models due to the strong variations in these ratios as a function of temperature in the collisionally ionized gas. At low temperatures, the C IV/C III ratio in our multiphase models is nearly the same as the QSOs+galaxies UVB photoionization model. However, for temperatures $\log T \gtrsim 5.3$, this ratio is ~ 2 to 15 times higher for the multiphase models than the photoionization models. Conversely, the C IV/O VI ratio is within a factor of two for both models at $\log T \gtrsim 5.3$, while at lower temperatures the multiphase models predict a C IV/O VI ratio factors of $\sim$4 to $>$1000 higher than the pure photoionization models (which give $N(\mathrm{C\ IV})/N(\mathrm{O\ VI}) \sim 0.6$ to 0.2 for the QSOs and QSOs+galaxies UVB, respectively). This large difference in models at low temperatures is due to the strong fall off in O VI ionization fraction with decreasing temperature over this range. These large differences for models in which a small fraction of the gas is associated with the collisionally-ionized phase is due to the very large (or small) ratios of C IV compared with the other two ions in collisionally ionized gas. For example, at $\log T = 5.45$, the C IV/C III ratio in CIE is expected to be $\sim$60 compared with $\sim$2 in the QSOs+galaxies photoionization model. Thus, even though the collisionally ionized phase is limited to $\lesssim 50\%$ of the total hydrogen at this temperature (see Figure 9), it contributes $> 90\%$ of the C IV.

Danforth & Shull (2008) studied the integrated column densities of C III, C IV, and O VI for a number of absorbers, finding C III/C IV ratios of ~ 1 and C IV/O VI ratios consistent with ~ 0.25 (both with a quite large scatter). Both of these ratios are consistent with our photoionization models, though it may be dangerous to draw conclusions based on these two average ratios, which rely on different samples of absorbers, without attempting models of the ionization to match the full range of ionization states in each absorber.

Indeed, Danforth & Shull conclude that the O VI mostly arises in collisionally-ionized gas on the basis of their comparisons. Danforth & Shull note that the correlation of C IV with both O VI and C III is not particularly strong, and they use this to argue that the observed C IV in their sample may arise from both shock-heated and photoionized gas (traced by O VI and C III, respectively, in their argument). A significant population of multiphase absorbers where the mixture of phases varies could presumably also provide for such a lack of correlation.

Future observations with the Cosmic Origins Spectrograph (COS) on board *HST* should provide significantly higher signal-to-noise ratio observations of QSOs than have been possible with STIS, albeit at lower spectral resolution. This can provide better limits and detections of weak absorption lines for some sight lines with quite low-S/N STIS observations, such as the PKS 0405–123 sight line, allowing stronger constraints on the models. In the present absorber, for example, O III already provides important constraints on the single-phase collisional ionization models. Better observations of this transition will begin to limit the photoionization and multiphase models more severely.

The metallicity of this absorber is quite high for both UVB spectra adopted here. There are significant systematic uncertainties associated with our estimates, but [O/H] ~ -0.6 or -0.15 are both high compared with the canonical mean of [O/H] -1. The high metallicity and great strength of the O VI absorption both favor an origin of this absorber near to a galaxy, although the H I column and estimated densities are not large. Given the discussion in the previous section, if this absorber were associated with a galaxy, it would likely be a sub-L_* system.

6 SUMMARY

We have presented *FUSE* and *HST*/STIS ultraviolet absorption line observations of the $z = 0.495096$ absorber toward the QSO PKS 0405–123. We have measured the column densities of H I, C III, N IV, O IV, O V, and O VI and placed upper limits on the column densities of another seven ions. We use these measurements to study the ionization processes at work in this absorber and estimate its metallicity.

The most important results of our work are as follows.

(i) This absorber shows very strong O VI absorption with no detectable Ne VIII or Mg X. There is no direct evidence for a strong component of gas with temperatures $T \gtrsim 5 \times 10^5$ K as expected if it traces the largest mass of missing baryons in a WHIM. However, the limits to the amount of material depend strongly on the temperature (see Figure 10). This system would not likely be detectable in X-ray absorption.

(ii) We have modeled the broad range of ions covered by our data using a number of collisional ionization and photoionizations models. This absorber can be modelled as purely photoionized gas with [O/H] ~ -0.6 if the ionizing UVB includes a significant contribution from photons associated with star forming galaxies and [O/H] ~ -0.15 if the UVB does not include a significant contribution from galaxies. These metallicities are robust to the inclusion of a collisionally ionized phase.

(iii) The ionization of the absorber may also be well described by multiphase models in which the photoionized gas in the absorber

is complemented by a contribution from hot ($T \gtrsim 3 \times 10^5$ K), collisionally ionized gas. The strong O VI in this system may trace a photoionized phase, a collisionally-ionized phase, or a mixture of both. In this case, the metallicities are still consistent with those from a pure photoionization model.

(iv) The uncertainties in the spectral shape of the ionizing UVB give rise to significant systematic uncertainties in the derived metallicity of the absorber, of order 0.5 dex or a factor of 3 in this case. Such uncertainties should be fully considered when studying the metallicity distribution, ionization, and baryon content derived from metal lines of the low-z IGM.

ACKNOWLEDGMENTS

We thank A.J. Fox, J.M. Shull, and T.M. Tripp for comments that improved our work. JCH and JXP recognize support from NASA grant NAG5-12345. JXP acknowledges support from NASA grant NAG5-12743. JCH and NL also recognize support from NASA grant NNX08AJ51G.

REFERENCES

Aguirre A., Dow-Hygelund C., Schaye J., Theuns T. 2008, ApJ, in press (astro-ph/0712.1239)
Aracil B., Tripp T.M., Bowen D.V., Prochaska J.X., Chen H.-W., Frye B.L. 2006, MNRAS, 367, 139
Asplund M. 2005, ARAA, 43, 481
Asplund M., Grevesse N., Sauval A.J. 2005a, in "Cosmic Abundances as Records of Stellar Evolution and Nucleosynthesis", ASP Conference Series, Vol. 336, Eds. T.G. Barnes and F. Bash, p. 25
Asplund M., Grevesse N., Sauval A.J., Allende Prieto C., Blomme R. 2005b, A&A, 431, 693
Asplund M., Grevesse N., Sauval A.J., Allende Prieto C., Kiselman D. 2004, A&A 417, 751
Ayres T. 2008, ApJ, 686, 731
Bahcall J.N., Basu, S., Pinsonneault, M., Serenelli, A.M. 2005, ApJ, 618, 1049
Bahcall J.N., Jannuzi B.T, Schneider D.P., Hartig G.F. 1993, ApJ, 405, 491
Basu S., Antia, H.M. 2008, PhysRpt, 457, 217
Bechtold J., et al. 2002, ApJS, 140, 143
Bennett C.L., et al. 2003, ApJS, 148, 97
Bertrone S., Schaye J., Dolag K. 2008, SSRv, 134, 295
Bregman J.N. 2007, ARAA 45, 221
Burles S., Tytler D. 1996, ApJ, 460, 584
Burles S., Tytler D. 1998, ApJ, 507, 732
Caffau, E., Ludwig, H.G., Steffen, M., Ayres, T.R., Bonifacio, P., Cayrel, R., Freytag, B., Plez, B. 2008, A&A, 488, 1031
Caffau, E., Maiorca, E., Bonifacio, P., Faraggiana, R., Steffen, M., Ludwig, H.G., Kamp, I., Busso, M. 2009, A&A, submitted
Calura F., Matteucci F. 2006, MNRAS, 369, 465
Cen R., Fang, T. 2006, ApJ, 650, 573
Cen R., Ostriker J.P. 1999, ApJ, 514, 1
Cen R., Ostriker J.P. 2006, ApJ, 650, 560
Cen, R., Tripp, T.M., Ostriker, J.P., Jenkins, E.B. 2001, ApJ, 559, L5
Chen H.-W., Prochaska J.X. 2000, ApJ, 543, L9
Cooksey K.L, Prochaska J.X., Chen H.-W., Mulchaey J.S., Weiner B.J. 2008, ApJ, 676, 262
Däppen, W. 2000, in "Allen's Astrophysical Quantities," Ed. A.N. Cox (Springer: New York), p. 27
Danforth, C.W. 2009, in "Future Directions in Ultraviolet Spectroscopy," Ed. M.E. Van Steenberg (astro-ph:0812.0602)
Danforth C.W., Shull J.M. 2005, ApJ, 624, 555
Danforth C.W., Shull J.M. 2008, ApJ, 679, 194
Danforth C.W., Shull J.M., Rosenberg J.L., Stocke J.T. 2006, ApJ, 640, 716
Davé R., et al. 2001, ApJ, 552, 473
Davé R., Oppenheimer, B.D. 2007, MNRAS, 374, 427
Davé R., Hernquist L., Katz N., Weinberg D.H. 1999, ApJ, 511, 521
Delahaye, F., Pinsonneault, M.H. 2006, ApJ, 649, 529
Dixon W.V., et al. 2007, PASP, 119, 527
Fang T., Bryan G.L. 2001, ApJ, 561, L31
Fang T., Canizares C.R., Yao Y. 2007, ApJ, 670, 992
Fang, T., Marshall, H. L., Lee, J. C., Davis, D. S., Canizares, C. R. 2002, ApJ, 572, L127
Faucher-Giguère C.-A., Lidz A., Hernquist L., Zaldarriaga M. 2008, ApJ, in press (astro-ph/0806.0372)
Ferland G.J., et al 1998, PASP, 110, 761
Fox, A.J., Wakker, B.P., Savage, B.D., Tripp, T.M., Sembach, K.R., Bland-Hawthorn, J. 2005, ApJ, 630, 332
Freedman W.L. et al. 2001, ApJ, 553, 47
Fukugita M. 2003, in Dark Matter in Galaxies, IAU Symp. 220, p. 194
Fukugita M., Hogan C.J., Peebles P.J.E. 1998, ApJ, 503, 518
Ganguly R., Cen R., Fang T., Sembach K. 2008, ApJ, 678, L89
Giroux, M.L., Shull, J.M. 1997, AJ, 113, 1505x
Grevesse, N., & Sauval, A.J. 1998, SSRv, 85, 161
Haardt F., Madau P. 2001, preprint (astro-ph/0106018)
Haardt F., Madau P. 1996, ApJ, 461, 20
Heckman T.M., Norman C.A., Strickland D.K., Sembach K.R. 2002, ApJ, 577, 691
Jenkins E.B., Tripp T.M. 2001, ApJS, 137, 297
Kang H., Ryu D., Cen R., Song D. 2005, ApJ, 620, 21
Kim Quijano J., et al. 2003, STIS Instrument Handbook, Version 7.0, (Baltimore: STScI)
Kirkman D., Tytler D., Suzuki N., O'Meara J.M., Lubin D. 2003, ApJS, 149, 1
Kriss G.A., et al. 2001, Science, 293, 1112
Lehner N., Prochaska J.X., Kobulnicky H.A., Cooksey K.L., Howk J.C., Williger G.M., Cales S.L. 2008, ApJ, submitted.
Lehner N., Savage B.D., Richter P., Sembach K.R., Tripp T.M., Wakker B.P. 2007, ApJ, 658, 680
Lehner N., Savage B.D., Wakker B.P., Sembach K.R., Tripp T.M. 2006, ApJS, 164, 1
Lodders, K. 2003, ApJ, 591, 1220
Lodders, K., Palme, H., Gail, H.-P. 2009, (astro-ph:0901.1149)
Ludwig, H.G., Steffen, M., in Precision Spectroscopy in Astrophysics, eds. N.C. Santos, L. Pasquini, A.C.M. Correia, M. Romanielleo, (Garching, Germany) 133
Mathews W.G., Ferland G.J. 1987, 323, 456
Melendez, J., Asplund, M. 2008, A&A, 490, 817
Morton D.C. 2003, ApJS, 149, 205
Mulchaey J.S., Mushotzky R.F., Burstein D., Davis D.S. 1996, ApJ, 456, L5
O'Meara J.M., Burles S., Prochaska J.X., Prochter G.E., Bernstein R.A., Burgess K.M. 2006, ApJ, 649, L61
O'Meara J.M., Tytler, D., Kirkman D., Nao S., Prochaska J.X., Lubin D., Wolfe A.M. 2001, ApJ, 522, 718

Oppenheimer, B.D., & Davé, R.A. 2009, MNRAS, in press (astro-ph/0806.2866)
Penton S.V., Stocke J.T., Shull J.M. 2004, ApJS, 152, 29
Pettini, M., Zych, B.J., Steidel, C.C., Chaffee, F.H. 2008, MNRAS, 385, 2011
Prochaska J.X., Chen H.-W., Howk J.C., Weiner B., Mulchaey J. 2004, ApJ, 617, 718
Prochaska J.X., Weiner B.J., Chen H.-W., Mulchaey J.S. 2006, ApJ, 643, 680
Richter P., Paerels F.B.S., Kaastra J.S. 2008, SSRv, 134, 25
Richter P., Savage B.D., Sembach K.R., Tripp T.M. 2004, ApJS, 153, 16
Savage B.D., Sembach K.R., Tripp T.M., Richter P. 2002, ApJ, 564, 631
Schaye J. 2001, 559, 507
Scott, P.C., Asplund, M., Grevesse, N., Sauval, A.J. 2006, A&A, 456, 675
Sembach K.R., Tripp T.M., Savage B.D., Richter P. 2004, ApJS, 155, 351
Shull, J.M., Tumlinson, J., Giroux, M.L. 2003, ApJ, 594, L107
Shull, J.M., Tumlinson, J., Giroux, M.L., Kriss, G.A., Reimers, D. 2004, ApJ, 600, 570
Simcoe R.A., Sargent W.L.W., Rauch M. 2004, ApJ, 606, 92
Simcoe R.A., Sargent W.L.W., Rauch M., Becker G. 2006, ApJ, 637, 648
Stocke J.T., Penton S.V., Danforth C.W., Shull J.M., Tumlinson J., McLin K.M. 2006, ApJ, 641, 217
Sutherland R.S., Dopita M.A. 1993, ApJS, 88, 253
Telfer R.C., Kriss G.A., Zheng W., Davidsen A.F., Tytler D. 2002, ApJ, 579, 500
Thom C., Chen H.-W. 2008a, ApJ, 683, 22
Thom C., Chen H.-W. 2008b, ApJ, 179, 37
Tripp T.M., Aracil B., Bowen D.V., Jenkins E.B. 2006, ApJ, 643, L77
Tripp T.M., Giroux M.L., Stocke J.T., Tumlinson J., Oegerle W.R. 2001, ApJ, 563, 724
Tripp T.M., et al. 2002, ApJ, 575, 697
Tripp T.M., Savage B.D. 2000, ApJ, 542, 42
Tripp T.M., Savage B.D., Jenkins E.B. 2000, ApJ, 534, L1
Tripp T.M., Sembach K.R., Bowen D.V., Savage B.D., Jenkins E.B., Lehner N., Richter P. 2008, ApJS, 177, 39
Tumlinson J., Shull J.M., Giroux M.L., Stocke J.T. 2005, ApJ, 620, 95
Verner D.A., Barthel P.D., Tytler D. 1994a, A&AS, 108, 287
Verner D.A., Tytler D., Barthel P.D. 1994b, ApJ, 430, 186
Wakker B.P., Savage B.D. 2008, ApJS, submitted.
Wiersma R.P.C., Schaye J., Smith B.D. 2008, MNRAS, 393, 99
Williams R.J., Mathur S., Nicastro F. 2006, ApJ, 645, 179
Williger G., Heap S.R., Weymann R.J., Davé R., Ellingson E., Carswell R.F., Tripp T.M., Jenkins E.B. 2006, ApJ, 636, 631
Zheng, W., Kriss, G.A., Telfer, R.C., Grimes, J.P., Davidsen, A.F. 1998, ApJ, 492, 855

This paper has been typeset from a TEX/ LATEX file prepared by the author.